Systematic study of relativistic and chemical enhancements of $\mathcal{P}, \mathcal{T}$-odd effects in polar diatomic radicals

Konstantin Gaul,[1,*] Sebastian Marquardt,[1] Timur Isaev,[2] and Robert Berger[1,†]

[1]*Fachbereich Chemie, Philipps-Universität Marburg, Hans-Meerwein-Straße 4, 35032 Marburg, Germany*

[2]*NRC "Kurchatov Institute" - Petersburg Nuclear Physics Institute by B.P. Konstantinov, Orlova Roscha. 1, 188300 Gatchina, Russia*

(Received 19 June 2018; published 21 March 2019)

Polar diatomic molecules that have, or are expected to have, a $^2\Sigma_{1/2}$-ground state are studied systematically with respect to simultaneous violation of parity $\mathcal{P}$ and time-reversal $\mathcal{T}$ with numerical methods and analytical models. Enhancements of $\mathcal{P}, \mathcal{T}$-violating effects due to an electric dipole moment of the electron (eEDM) and $\mathcal{P}, \mathcal{T}$-odd scalar-pseudoscalar nucleon-electron current interactions are analyzed by comparing trends within columns and rows of the periodic table of the elements. For this purpose electronic structure parameters are calculated numerically within a quasirelativistic zeroth order regular approximation (ZORA) approach in the framework of complex generalized Hartree-Fock (cGHF) or Kohn-Sham (cGKS). Scaling relations known from analytic relativistic atomic structure theory are compared to these numerical results. Based on this analysis, problems of commonly used relativistic enhancement factors are discussed. Furthermore, the ratio between both $\mathcal{P}, \mathcal{T}$-odd electronic structure parameters mentioned above is analyzed for various groups of the periodic table. From this analysis an analytic measure for the disentanglement of the two $\mathcal{P}, \mathcal{T}$-odd electronic structure parameters with multiple experiments in dependence of electronic structure enhancement factors is derived.

DOI: 10.1103/PhysRevA.99.032509

I. INTRODUCTION

Simultaneous violation of space ($\mathcal{P}$) and time ($\mathcal{T}$) parity in the charged lepton sector is considered to be a strong indicator for physics beyond the standard model of particle physics [1]. Exploiting enhancement effects in bound systems, such as atoms or molecules, low-energy experiments actually provide the best limits on $\mathcal{P}, \mathcal{T}$ violation in this sector and thus are among the most useful tools to exclude new physical theories and to test the standard model [2,3].

Understanding these atomic and molecular enhancement effects in detail is essential for the development of experiments sensitive to $\mathcal{P}, \mathcal{T}$ violation.

A permanent atomic or molecular electric dipole moment (EDM) that causes a linear Stark shift in the limit of zero external fields would violate $\mathcal{P}, \mathcal{T}$ [3]. Mainly four sources of a permanent EDM are commonly considered for molecules: permanent electric dipole moments of the nuclei, $\mathcal{P}, \mathcal{T}$-odd nucleon-nucleon current interactions, a permanent electric dipole moment of the electron (eEDM), and $\mathcal{P}, \mathcal{T}$-odd nucleon-electron current interactions (see, e.g., [4]). Of these sources the latter two have the most important contribution in paramagnetic systems [4]. Furthermore, in open-shell molecules nucleon-electron interactions are expected to be dominated by scalar-pseudoscalar interactions that are nuclear spin independent.

Since the formulation of an eEDM interaction Hamiltonian for atoms by Salpeter in the year 1958 [5], there have been many studies on eEDM enhancement in atoms and molecules. Sandars worked out analytical relations of atomic eEDM interactions in the 1960s [6–9], which were confirmed also by others [10,11]. Sandars calculated that the enhancement of the eEDM in atoms scales with $\alpha^2 Z^3$, where α is the fine-structure constant and Z is the nuclear charge number. Enhancements of scalar-pseudoscalar nucleon-electron current interactions in atoms scale as αZ^3 [12]. Since then, a number of numerical studies was conducted, but most of the previous investigations focused on the description of $\mathcal{P}, \mathcal{T}$-odd effects in individual or few molecular candidates.

Some attempts were made to obtain a deeper understanding of enhancement of $\mathcal{P}, \mathcal{T}$-odd effects in molecules beyond established Z-dependent scaling laws: In Ref. [13], for instance, the influence of the nuclear charge number of the electronegative partner on eEDM enhancements in mercury monohalides was studied. Furthermore, effects of the polarization of the molecule by the electronegative partner on the eEDM enhancement are discussed. In Ref. [13] it was concluded that the nuclear charge of the lighter halogen atom influences the eEDM enhancement less than its electronegativity.

Recently Sunaga *et al.* studied large eEDM enhancement effects in hydrides within orbital interaction theory and remarked an influence of the energy difference between the interacting valence orbitals of the electronegative atom and the unoccupied $p_{1/2}$ orbital of the heavy atom [14]. Both of the mentioned studies confirmed that large contributions of s- and p-type atomic orbitals in the singly occupied molecular orbital increase $\mathcal{P}, \mathcal{T}$-odd effects, as predicted in Ref. [12]. A similar result was obtained by Ravaine *et al.* in 2005 [15], who showed that the covalent character of HI^+ causes a stronger s-p mixing and therefore a larger enhancement of the eEDM than in ionically bound HBr^+.

[*]Parts of this work were reported in preliminary form in the M.Sc. thesis of Konstantin Gaul.

[†]robert.berger@uni-marburg.de

The majority of previous studies on $\mathcal{P},\mathcal{T}$-violating effects in molecules were performed within a four-component (relativistic) framework. Our recently developed two-component (quasirelativistic) approach for the calculation of $\mathcal{P},\mathcal{T}$-odd effects [16] allows for routine calculations of a large number of molecules on an *ab initio* level. In this paper we study diatomic radicals systematically across the periodic table, which are known to have a $^2\Sigma_{1/2}$-ground state, or for which at least a $^2\Sigma_{1/2}$-ground state is naively expected from simple chemical bonding concepts. In combination with analytic scaling relations, we calculate the Z-dependent and Z-independent electronic structure effects in different groups of the periodic table. Furthermore, we gauge the "chemical" influences on the $\mathcal{P},\mathcal{T}$-odd enhancement particularly using an analysis of isolobal diatomic molecules, i.e., changes in the enhancement throughout the columns of the periodic table.

Herewith, we provide a consistent overview of $\mathcal{P},\mathcal{T}$-odd effects in a large number of diatomic molecules, which may serve as a suitable starting point for further research with higher-level electronic structure methods, where needed. By analyzing general trends of the ratio between molecular enhancement factors of the eEDM and nucleon-electron current interactions, we draw conclusions on their possible disentanglement in experiments with polar diatomic radicals that feature a $^2\Sigma_{1/2}$-ground state.

II. THEORY

In this section we shortly introduce the employed Hamiltonians used for calculations of $\mathcal{P},\mathcal{T}$-odd effects in diatomic molecules in order to clarify their limitations. Additionally, we give an overview of relativistic enhancement effects in the herein studied properties, which are important for the following discussions. Finally, we present neglected many-electron and magnetic effects that may significantly influence the performed studies of $\mathcal{P},\mathcal{T}$-odd effects in molecules without heavy elements.

A. $\mathcal{P},\mathcal{T}$-odd spin-rotational Hamiltonian

We present herein electronic structure calculations for polar diatomic molecules that are expected to have a $^2\Sigma_{1/2}$-ground state. For these systems an effective spin-rotational Hamiltonian can be derived that in particular describes a transition of Hund's coupling case (c) to case (b) [17–19]. This corresponds to cases where the rotational constant is much smaller than the spin-doubling constant but much larger than the Ω-doubling constant (for details see Ref. [20]). The $\mathcal{P},\mathcal{T}$-odd part of this effective spin-rotational Hamiltonian reads (see, e.g., Refs. [20,21])

$$H_{\mathrm{sr}} = (k_{\mathrm{s}} W_{\mathrm{s}} + d_{\mathrm{e}} W_{\mathrm{d}})\Omega = W_{\mathrm{d}}(k_{\mathrm{s}} W_{\mathrm{s}}/W_{\mathrm{d}} + d_{\mathrm{e}})\Omega, \tag{1}$$

where $\Omega = \vec{J}_{\mathrm{e}} \cdot \vec{\lambda}$ is the projection of the reduced total electronic angular momentum $\vec{J}_{\mathrm{e}}$ on the molecular axis, defined by the unit vector $\vec{\lambda}$ pointing from the heavy to the light nucleus. k_{s} is the $\mathcal{P},\mathcal{T}$-odd scalar-pseudoscalar nucleon-electron current interaction constant and d_{e} is the eEDM. The $\mathcal{P},\mathcal{T}$-odd electronic structure parameters are defined by

$$W_{\mathrm{s}} = \frac{\langle \Psi \,|\, \hat{H}_{\mathrm{s}} \,|\, \Psi \rangle}{k_{\mathrm{s}}\Omega}, \tag{2a}$$

$$W_{\mathrm{d}} = \frac{\langle \Psi \,|\, \hat{H}_{\mathrm{d}} \,|\, \Psi \rangle}{d_{\mathrm{e}}\Omega}, \tag{2b}$$

where Ψ is the electronic wave function and the molecular $\mathcal{P},\mathcal{T}$-odd Hamiltonians are [3,5]

$$\hat{H}_{\mathrm{s}} = \imath k_{\mathrm{s}} \frac{G_{\mathrm{F}}}{\sqrt{2}} \sum_{i=1}^{N_{\mathrm{elec}}} \sum_{A=1}^{N_{\mathrm{nuc}}} \rho_A(\vec{r}_i) Z_A \boldsymbol{\gamma}^0 \boldsymbol{\gamma}^5, \tag{3}$$

$$\hat{H}_{\mathrm{d}} = -d_{\mathrm{e}} \sum_{i=1}^{N_{\mathrm{elec}}} (\boldsymbol{\gamma}^0 - \mathbf{1}_{2\times 2}) \vec{\boldsymbol{\Sigma}} \cdot \vec{\mathcal{E}}(\vec{r}_i). \tag{4}$$

In this equation $\hat{H}_{\mathrm{d}}$ refers to $\hat{H}_{\mathrm{d,I}}$, obtained according to stratagem I by commuting the unperturbed Dirac-Coulomb Hamiltonian with a modified momentum operator as reported in Ref. [22]. In the following the index I is only used, when we compare to other forms of the Hamiltonian. If no additional index (I, II, or other) is used we refer always to $\hat{H}_{\mathrm{d,I}}$. Here the sums run over all N_{elec} electrons and all N_{nuc} nuclei, ρ_A is the normalized nuclear density distribution of nucleus A with charge number Z_A, $\vec{r}_i$ is the position vector of electron i, $\vec{\mathcal{E}}$ is the internal electrical field, $G_{\mathrm{F}} = 2.22249 \times 10^{-14}\ E_{\mathrm{h}} a_0^3$ is Fermi's weak coupling constant, $\imath = \sqrt{-1}$ is the imaginary unit, and the Dirac matrices in standard notation are defined as ($k = 1, 2, 3$)

$$\begin{aligned} \boldsymbol{\gamma}^0 &= \begin{pmatrix} \mathbf{1}_{2\times 2} & \mathbf{0}_{2\times 2} \\ \mathbf{0}_{2\times 2} & -\mathbf{1}_{2\times 2} \end{pmatrix}, \quad \boldsymbol{\gamma}^k = \begin{pmatrix} \mathbf{0}_{2\times 2} & \boldsymbol{\sigma}^k \\ -\boldsymbol{\sigma}^k & \mathbf{0}_{2\times 2} \end{pmatrix}, \\ \boldsymbol{\gamma}^5 &= \begin{pmatrix} \mathbf{0}_{2\times 2} & \mathbf{1}_{2\times 2} \\ \mathbf{1}_{2\times 2} & \mathbf{0}_{2\times 2} \end{pmatrix}, \quad \boldsymbol{\Sigma}^k = \begin{pmatrix} \boldsymbol{\sigma}^k & \mathbf{0}_{2\times 2} \\ \mathbf{0}_{2\times 2} & \boldsymbol{\sigma}^k \end{pmatrix}, \end{aligned} \tag{5}$$

with the vector of the Pauli spin matrices $\vec{\boldsymbol{\sigma}}$. For better readability we have dropped all electron indices on Dirac and Pauli matrices as these are in the present discussion only referred to as the electron with index i.

In this work the electronic structure parameters were calculated, using the corresponding quasirelativistic Hamiltonians within the zeroth order regular approximation (ZORA) [16,23,24]

$$\hat{H}_{\mathrm{s}}^{\mathrm{ZORA}} = \imath \sum_{i=1}^{N_{\mathrm{elec}}} \sum_{A=1}^{N_{\mathrm{nuc}}} Z_A [\rho_A(\vec{r}_i)\tilde{\omega}_{\mathrm{s}}(\vec{r}_i), \vec{\boldsymbol{\sigma}} \cdot \hat{\vec{p}}_i]_-, \tag{6}$$

$$\hat{H}_{\mathrm{d}}^{\mathrm{ZORA}} = \sum_{i=1}^{N_{\mathrm{elec}}} (\vec{\boldsymbol{\sigma}} \cdot \hat{\vec{p}}_i)\tilde{\omega}_{\mathrm{d}}(\vec{r}_i)\vec{\boldsymbol{\sigma}} \cdot \vec{\mathcal{E}}(\vec{r}_i)(\vec{\boldsymbol{\sigma}} \cdot \hat{\vec{p}}_i), \tag{7}$$

where $\hat{\vec{p}}$ is the linear momentum operator, $[A, B]_- = AB - BA$ is the commutator, and the modified ZORA factors are defined as

$$\tilde{\omega}_{\mathrm{s}}(\vec{r}_i) = \frac{G_{\mathrm{F}} k_{\mathrm{s}} c}{\sqrt{2}[2m_{\mathrm{e}}c^2 - \tilde{V}(\vec{r}_i)]}, \tag{8}$$

$$\tilde{\omega}_{\mathrm{d}}(\vec{r}_i) = \frac{2d_{\mathrm{e}}c^2}{[2m_{\mathrm{e}}c^2 - \tilde{V}(\vec{r}_i)]^2}\ , \tag{9}$$

with the model potential $\tilde{V}$ introduced by van Wüllen [25], which is used to alleviate the gauge dependence of ZORA. Here c is the speed of light in vacuum and m_e is the mass of the electron. The internal electrical field can be approximated as the field of the nuclei [16,22]:

$$\vec{\mathcal{E}}(\vec{r}_i) \approx \sum_{A=1}^{N_{\rm nuc}} k_{\rm es} Z_A e \frac{\vec{r}_i - \vec{r}_A}{|\vec{r}_i - \vec{r}_A|^3}, \tag{10}$$

with e being the elementary charge and the constant $k_{\rm es}$ being $(4\pi\epsilon_0)^{-1}$ in SI units with the electric constant ϵ_0.

For heavy elements, however, finite size effects of the nucleus can play a crucial role for the description of the internal electric field. The internal electrical field generated by a Gaussian shaped nucleus is described by

$$\vec{\mathcal{E}}(\vec{r}_i) \approx \sum_{A=1}^{N_{\rm nuc}} \frac{k_{\rm es} Z_A e}{|\vec{r}_i - \vec{r}_A|^2} \left[\frac{\mathrm{erf}(\sqrt{\zeta_A}|\vec{r}_i - \vec{r}_A|)}{|\vec{r}_i - \vec{r}_A|} - 2\left(\frac{\zeta_A}{\pi}\right)^{1/2} \exp(-\zeta_A |\vec{r}_i - \vec{r}_A|^2) \right] (\vec{r}_i - \vec{r}_A), \tag{11}$$

where $\zeta_A = \frac{3}{2r_{{\rm nuc},A}^2}$ and the root mean square radius $r_{{\rm nuc},A}$ of nucleus A was used as suggested by Visscher and Dyall [26].

An alternative expression for the eEDM interaction Hamiltonian, including two-electron interactions implicitly, denoted as stratagem II in Ref. [22], can be derived [27]:

$$\hat{H}_{\rm d,II} = \frac{2\imath c d_e}{\hbar e} \sum_{i=1}^{N_{\rm elec}} \boldsymbol{\gamma}^0 \boldsymbol{\gamma}^5 \hat{\vec{p}}_i^2. \tag{12}$$

In this form of the eEDM-Hamiltonian effects due to the finite size of the nuclei are considered implicitly, if the wave function of electrons moving in the potential of a finite nucleus is employed. The corresponding ZORA-Hamiltonian is given by [16]

$$\hat{H}_{\rm d,II}^{\rm ZORA} = \sum_{i=1}^{N_{\rm elec}} \left[\imath \hat{\vec{p}}_i^2 \omega_{\rm d,II}(\vec{r}_i)(\vec{\boldsymbol{\sigma}} \cdot \hat{\vec{p}}_i) - \imath (\vec{\boldsymbol{\sigma}} \cdot \hat{\vec{p}}_i) \omega_{\rm d,II}(\vec{r}_i) \hat{\vec{p}}_i^2 \right], \tag{13}$$

where the modified ZORA factor is defined as

$$\omega_{\rm d,II}(\vec{r}_i) = \frac{2 d_e c^2}{2e\hbar m_e c^2 - e\hbar \tilde{V}(\vec{r}_i)}. \tag{14}$$

Furthermore, the total angular momentum projection was calculated explicitly by

$$\Omega = \left(\langle \Psi_{\rm ZORA} \,|\, \sum_i \hat{\vec{\ell}}_i \,|\, \Psi_{\rm ZORA} \rangle + \frac{1}{2} \langle \Psi_{\rm ZORA} \,|\, \sum_i \vec{\boldsymbol{\sigma}}_i \,|\, \Psi_{\rm ZORA} \rangle \right) \cdot \vec{\lambda}, \tag{15}$$

where $\hat{\vec{\ell}}_i$ is the reduced orbital angular momentum operator for electron i and $\Psi_{\rm ZORA}$ is the ZORA multielectron wave function.

B. Scaling relations of $\mathcal{P}, \mathcal{T}$-odd properties

Within the relativistic Fermi-Segrè model for electronic wave functions [28] the matrix elements of the $\mathcal{P}, \mathcal{T}$-odd operators can be obtained analytically for atomic systems [12,29]. The results for the $\mathcal{P}, \mathcal{T}$-odd nucleon-electron current interactions can be expressed in terms of a relativistic enhancement factor

$$R(Z, A) = \frac{4}{\Gamma^2(2\gamma + 1)} (2Z r_{\rm nuc}/a_0)^{2\gamma - 2}, \tag{16}$$

where $\Gamma(z)$ is the gamma function, Z and A are the nuclear charge and mass numbers, respectively, $r_{\rm nuc} \approx 1.2\ \mathrm{fm}\ A^{1/3}$ is the nuclear radius, a_0 is the Bohr radius, and

$$\gamma = \sqrt{\left(j + \frac{1}{2}\right)^2 - (\alpha Z)^2}, \tag{17}$$

with the fine structure constant $\alpha \approx \frac{1}{137}$ and the total electronic angular momentum quantum number j.

In terms of the relativistic enhancement the parameters of the $\mathcal{P}, \mathcal{T}$-odd spin-rotational Hamiltonian can now be estimated to behave as (see Ref. [12] for W_s and Refs. [11,30] for W_d)

$$W_s \approx -\frac{G_F}{2\pi\sqrt{2}a_0^3} \underbrace{R(Z, A)\gamma}_{R_s(Z,A)} Z^3 \alpha \varkappa, \tag{18}$$

$$W_d \approx -\frac{4E_h}{3e\,a_0} \underbrace{\frac{3}{\gamma(4\gamma^2 - 1)}}_{R_{\rm d,CS}(Z)} Z^3 \alpha^2 \varkappa, \tag{19}$$

where $\varkappa$ is a constant that depends on the effective electronic structure of the system under study. In relation (19) the label CS indicates that the factor was derived by Sandars [7] from a method by Casimir.

We note in passing that the relativistic enhancement factor of the eEDM induced permanent atomic EDM $R_{\rm d,CS}(Z)$ is the same as the one for hyperfine interactions published first by Racah in 1931 [31]: $R_{\rm d,CS}(Z) = R_{\rm hf,R}(Z)$. The denominator in relation (19) has two roots: one at $Z = \frac{\sqrt{j^2+j}}{\alpha}$ and one at $Z = \frac{\frac{1}{2}+j}{\alpha}$. Thus the relativistic enhancement factor causes problems not only for $Z > 137$ but diverges at $Z = \frac{\sqrt{3}}{2\alpha} \approx 118.65$ for ${}^2\Sigma_{1/2}$ states (see Fig. 1). This was also found by Dinh *et al.* in a study of hyperfine interactions in super heavy atoms [32]. These findings imply that relation (19) is of limited use to estimate W_d for elements with $Z > 100$.

An alternative relativistic enhancement factor for hyperfine interactions was found empirically by Fermi and Segrè [28,33], who interpolated numerically calculated data by Racah and Breit [31,34]:

$$R_{\rm hf,FS}(Z) = \frac{1}{\gamma^4}, \tag{20}$$

where the label FS was introduced referring to Fermi and Segrè. $R_{\rm hf,FS}(Z)$ has no singularities for $Z < 137$, and therefore no severe problems in the description of elements up to $Z \leqslant 118$ are expected. Furthermore, Eq. (20) can also be applied to estimate the eEDM enhancement, because the atomic

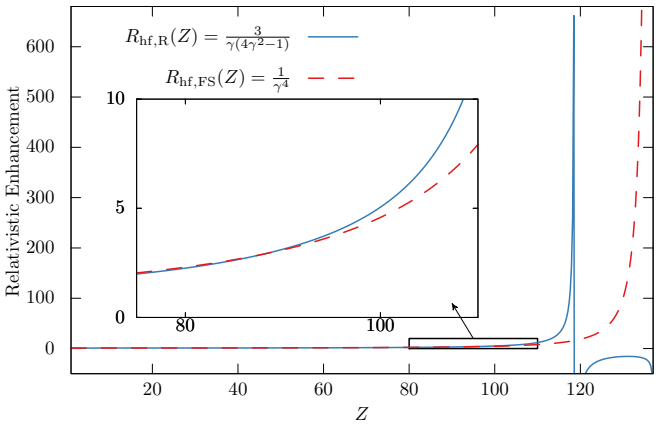

FIG. 1. Comparison of relativistic enhancement factors for eEDM induced permanent EDMs of atoms. Factor by Sandars derived analytically with Casimirs method (CS) and empirical factor for hyperfine interaction found by Fermi and Segrè (FS). Plots are shown for the case of $j = \frac{1}{2}$ as in $^2\Sigma_{1/2}$ states.

integrals relevant for the hyperfine structure and eEDM enhancement do not differ significantly within the Fermi-Segrè model and result in similar enhancement factors differing only by a factor of αZ (see also above and [7]):

$$R_{\mathrm{hf}}(Z) \sim \int dr\, r^{-2} g_0(r) f_0(r), \tag{21a}$$

$$R_{\mathrm{d}}(Z) \sim \int dr\, r^{-2} f_1(r) f_0(r), \tag{21b}$$

where g_ℓ and f_ℓ are the upper and lower component of the Dirac bispinor for a specific orbital angular quantum number ℓ, respectively. As $g_0(r)\alpha Z \approx f_1(r) +$ corrections, for hydrogenlike atoms, the integrals in Eqs. (21a) and (21b) are in a first approximation identical up to a factor of αZ. Thus the empirical factor (20) can be employed for our purposes (see also Fig. 1).

An improved relativistic enhancement factor for the $\mathcal{P},\mathcal{T}$-odd nucleon-electron current interaction parameter W_{s} was calculated with an analytical atomic model in [35]

$$W_{\mathrm{s}} \approx -\frac{G_{\mathrm{F}}}{2\pi\sqrt{2}a_0^3} Z^3 \alpha R(Z,A) f(Z) \frac{\gamma+1}{2} \varkappa, \tag{22}$$

with the Z-dependent function

$$f(Z) = \frac{1 - 0.56\alpha^2 Z^2}{(1 - 0.283\alpha^2 Z^2)^2}, \tag{23}$$

which results from a polynomial expansion of the atomic wave functions (see the Appendix of Ref. [35] for details).[1]

In Refs. [23,35] the eEDM enhancement parameter W_{d} was estimated from W_{s} by use of a relativistic enhancement factor for the ratio $W_{\mathrm{d}}/W_{\mathrm{s}}$ derived from Eqs. (22) and (19):

$$\tilde{R}_{\mathrm{CS}}(Z,A) = \frac{6}{\gamma(4\gamma^2-1)(\gamma+1) f(Z) R(Z,A)}. \tag{24}$$

In combination with summarized conversion factors and constant prefactors of W_{s} and W_{d}:

$$c_{\mathrm{conv}} = \frac{8\sqrt{2}\pi\alpha}{3\frac{G_{\mathrm{F}}\, e}{E_{\mathrm{h}} a_0^2}}, \tag{25}$$

an estimate for W_{d} is received from W_{s} via

$$W_{\mathrm{d}} \approx c_{\mathrm{conv}} \tilde{R}_{\mathrm{CS}}(Z,A) W_{\mathrm{s}}. \tag{26}$$

When relation (20) is used instead of (19), one obtains an alternative relativistic enhancement factor, which is expected to be more accurate for atoms with a high Z:

$$\tilde{R}_{\mathrm{FS}}(Z,A) = \frac{2}{\gamma^4(\gamma+1) R(Z,A) f(Z)}. \tag{27}$$

For comparison, instead of the improved relativistic factor for W_{s} [Eq. 22] relation (18) can be used to receive relativistic enhancement factors:

$$\tilde{\tilde{R}}_{\mathrm{CS}}(Z,A) = \frac{3}{\gamma^2(4\gamma^2-1) R(Z,A)}, \tag{28a}$$

$$\tilde{\tilde{R}}_{\mathrm{FS}}(Z,A) = \frac{1}{\gamma^5 R(Z,A)}. \tag{28b}$$

In the following discussion we will show that Eqs. (20) and (27) indeed agree much better with numerical calculations for $Z > 100$ than Eqs. (19) and (24), while there is no appreciable difference for molecules with lighter atoms.

C. Neglected many-electron effects in light molecules

In the approximation of the nuclear internal field [Eq. (10)] all $\mathcal{P},\mathcal{T}$-odd operators shown in Sec. II A are one-electron operators. Their expectation values scale with the nuclear charge number as Z^3. Thus these contributions are dominant in high-Z molecules. However, in light molecules many-electron effects with lower Z dependence stemming from the Hartree-Fock picture or the Breit interaction can have an important contribution to the enhancement factors, which we want to outline here for completeness, as our results reported for light molecules may be affected by this.

In the following we focus first on additional contributions in the Dirac-Hartree-Fock (DHF) picture that arise from the ZORA transformation. The DHF equation without magnetic fields and with perturbations (4) and (3) reads

$$\begin{pmatrix} \hat{V}_0(\vec{r})\mathbf{1}_{2\times2} - \hat{\mathbf{K}}_{\phi\phi} - \epsilon_i \mathbf{1}_{2\times2} & c\vec{\sigma}\cdot\hat{\vec{p}} - \hat{\mathbf{K}}_{\phi\chi} + \imath k_{\mathrm{s}} \frac{G_{\mathrm{F}}}{\sqrt{2}} \rho_{\mathrm{nuc}}(\vec{r})\mathbf{1}_{2\times2} \\ c\vec{\sigma}\cdot\hat{\vec{p}} - \hat{\mathbf{K}}_{\chi\phi} - \imath k_{\mathrm{s}} \frac{G_{\mathrm{F}}}{\sqrt{2}} \rho_{\mathrm{nuc}}(\vec{r})\mathbf{1}_{2\times2} & [\hat{V}_0(\vec{r}) - 2m_{\mathrm{e}}c^2]\mathbf{1}_{2\times2} - \hat{\mathbf{K}}_{\chi\chi} - \epsilon_i \mathbf{1}_{2\times2} + 2d_{\mathrm{e}}\vec{\sigma}\cdot\vec{\mathcal{E}}(\vec{r}) \end{pmatrix} \begin{pmatrix} \phi_i \\ \chi_i \end{pmatrix} = \begin{pmatrix} 0 \\ 0 \end{pmatrix}, \tag{29}$$

[1]The explicit numerical factors in $f(Z)$ were printed partially wrong in Ref. [35], which was mentioned in Ref. [23].

where ϕ_i and χ_i are the upper and lower components of the Dirac bispinor of orbital i, respectively, and ϵ_i is its orbital energy. The nuclear charge density is summarized as $\rho_{\text{nuc}}(\vec{r}) = \sum_{A=1}^{N_{\text{nuc}}} Z_A \rho_A(\vec{r})$ and $\hat{V}_0(\vec{r}) = \hat{V}_{\text{ext}}(\vec{r}) + \hat{V}_{\text{nuc}}(\vec{r}) + \hat{J}_{\phi\phi}(\vec{r}) + \hat{J}_{\chi\chi}(\vec{r})$ is the potential energy operator appearing on the diagonal, where $\hat{V}_{\text{ext}}$ and $\hat{V}_{\text{nuc}}$ are the external and nuclear potential energy operators, respectively. $\hat{J}_{\phi\phi}$ and $\hat{J}_{\chi\chi}$ are the direct parts and $\hat{\mathbf{K}}_{\phi\phi}$, $\hat{\mathbf{K}}_{\phi\chi}$, $\hat{\mathbf{K}}_{\chi\phi}$, $\hat{\mathbf{K}}_{\chi\chi}$ are the exchange parts that emerge from the two-electron Coulomb operator in DHF theory.

Whereas the direct Dirac-Coulomb contributions $\hat{J}_{\phi\phi}$ and $\hat{J}_{\chi\chi}$ are local and appear on the diagonal, the exchange contributions are nonlocal and nondiagonal

$$\hat{\mathbf{K}} = \begin{pmatrix} \hat{\mathbf{K}}_{\phi\phi} & \hat{\mathbf{K}}_{\phi\chi} \\ \hat{\mathbf{K}}_{\chi\phi} & \hat{\mathbf{K}}_{\chi\chi} \end{pmatrix}. \tag{30}$$

Thus when deriving an approximate relation between ϕ and χ, as when transforming into the ZORA picture, the exchange terms can result in additional contributions to the $\mathcal{P},\mathcal{T}$-odd enhancement.

We start our discussion with the scalar-pseudoscalar nucleon-electron current interaction Hamiltonian. The effective one-electron ZORA-Hamiltonian with this nucleon-electron current perturbation appears as

$$\begin{aligned} &\hat{h}_0^{\text{ZORA-HF}} + \hat{h}_{\text{s}}^{\text{ZORA-HF}} \\ &= \left(\vec{\boldsymbol{\sigma}} \cdot \hat{\vec{p}} - \frac{1}{c}\hat{\mathbf{K}}_{\phi\chi} + \imath k_{\text{s}} \frac{G_{\text{F}}}{c\sqrt{2}} \rho_{\text{nuc}} \mathbf{1}_{2\times 2}\right)\omega \\ &\quad \times \left(\vec{\boldsymbol{\sigma}} \cdot \hat{\vec{p}} - \frac{1}{c}\hat{\mathbf{K}}_{\chi\phi} - \imath k_{\text{s}} \frac{G_{\text{F}}}{c\sqrt{2}} \rho_{\text{nuc}} \mathbf{1}_{2\times 2}\right), \end{aligned} \tag{31}$$

where $\hat{h}_0^{\text{ZORA-HF}} = (\vec{\boldsymbol{\sigma}} \cdot \hat{\vec{p}} - \frac{1}{c}\hat{\mathbf{K}}_{\phi\chi})\omega(\vec{\boldsymbol{\sigma}} \cdot \hat{\vec{p}} - \frac{1}{c}\hat{\mathbf{K}}_{\chi\phi})$ is the unperturbed ZORA-Hamiltonian in the HF approximation and $\omega = \frac{c^2}{2m_{\text{e}}c^2 - \tilde{V}}$ is the ZORA factor with the model potential $\tilde{V}$. This results in additional correction terms to (6) stemming from the many-electron mean-field picture (only terms to first order in G_{F} are shown):

$$\Delta\hat{h}_{\text{s}}^{\text{ZORA-HF}} = \frac{1}{c}\rho_{\text{nuc}}\tilde{\omega}_{\text{s}}\hat{\mathbf{K}}_{\chi\phi} - \frac{1}{c}\hat{\mathbf{K}}_{\phi\chi}\tilde{\omega}_{\text{s}}\rho_{\text{nuc}}. \tag{32}$$

$\tilde{\omega}_{\text{s}}$ and the exchange operators $\hat{\mathbf{K}}_{\phi\chi}, \hat{\mathbf{K}}_{\chi\phi}$ are $O(\alpha)$, that is of order α, and therefore these correction terms are $O(\alpha^3)$, whereas the Hamiltonian defined in Eq. (3) is of first order in α.

We now focus on the eEDM interaction Hamiltonian. The ZORA transformation of the DHF operator using our method from [16] yields

$$\hat{h}_{\text{d}}^{\text{ZORA-HF}} = \left(\vec{\boldsymbol{\sigma}} \cdot \hat{\vec{p}} - \frac{1}{c}\hat{\mathbf{K}}_{\phi\chi}\right)(\tilde{\omega}_{\text{d}}\vec{\boldsymbol{\sigma}} \cdot \vec{\mathcal{E}})\left(\vec{\boldsymbol{\sigma}} \cdot \hat{\vec{p}} - \frac{1}{c}\hat{\mathbf{K}}_{\chi\phi}\right). \tag{33}$$

Thus many-electron mean-field correction terms to (7) are received as

$$\begin{aligned} \Delta\hat{h}_{\text{d}}^{\text{ZORA-HF}} = &-\frac{1}{c}\hat{\mathbf{K}}_{\phi\chi}\tilde{\omega}_{\text{d}}\vec{\boldsymbol{\sigma}} \cdot \vec{\mathcal{E}}\vec{\boldsymbol{\sigma}} \cdot \hat{\vec{p}} - \frac{1}{c}\vec{\boldsymbol{\sigma}} \cdot \hat{\vec{p}}\tilde{\omega}_{\text{d}}\vec{\boldsymbol{\sigma}} \cdot \vec{\mathcal{E}}\hat{\mathbf{K}}_{\chi\phi} \\ &+ \frac{1}{c^2}\hat{\mathbf{K}}_{\phi\chi}\tilde{\omega}_{\text{d}}\vec{\boldsymbol{\sigma}} \cdot \vec{\mathcal{E}}\hat{\mathbf{K}}_{\chi\phi}. \end{aligned} \tag{34}$$

The terms are sorted by their order in α. The first two terms are $O(\alpha^4)$ and the last term is $O(\alpha^6)$ and thus is suppressed. The first two terms are suppressed by a factor α^2 in comparison to the operator of Eq. (7). This is why the correction terms of Eqs. (32) and (34) have been neglected in the present study even when HF is used. For light elements, however, such terms can become more important, as has been shown, e.g., in Ref. [36].

In a density functional theory (DFT) picture none of the above terms $\Delta\hat{h}_{\text{d}}^{\text{ZORA-HF}}$, $\Delta\hat{h}_{\text{s}}^{\text{ZORA-HF}}$ arises if conventional nonrelativistic density functionals are used. Thus we would expect a larger deviation of HF-ZORA from DHF calculations than of Kohn-Sham (KS)-ZORA from Dirac-Kohn-Sham (DKS) calculations. However, if hybrid functionals are used as in our present paper, Fock exchange is considered explicitly and inclusion of the correction terms mentioned above may become necessary for light elements.

If the above discussed exchange terms become important, terms of comparatively low order in α, which have been neglected so far, may become important as well. These include the two-electron part of the internal electrical field

$$-\sum_{i<j}^{N_{\text{elec}}} k_{\text{es}} e\left(\boldsymbol{\gamma}_i^0 - \mathbf{1}_{2\times 2i}\right)\vec{\boldsymbol{\Sigma}}_i \cdot \frac{\vec{r}_i - \vec{r}_j}{|\vec{r}_i - \vec{r}_j|^3}\mathbf{1}_{2\times 2j}. \tag{35}$$

However, if the alternative effective one-electron form of the operator [Eq. (12)] is used, the two-electron contributions from the electric field can be included implicitly within a mean-field approach [27]. Our previous calculations [16] have shown that these effects are negligible. In our present study the effects for light molecules are below 5% and for super heavy elements below 1%, as can be seen in Sec. IV A, and are thus not important for the present discussion.

Another term of comparatively low order in α is the Breit contribution to the interaction with an eEDM, which was discussed in Ref. [22].

Additional corrections appear from the ZORA transformation, when the Breit interaction is considered, which appears as well on the off-diagonal elements of the Hamiltonian (see, e.g., [36]). These Breit interaction corrections appear for $\hat{H}_{\text{s}}$ as well.

For a more accurate calculation of the eEDM enhancement other magnetic terms $O(\alpha^2)$, which were neglected in the deviation in our previous paper [16], can play an important role as well and should be considered (see, e.g., [22]).

Beside the magnetic contributions, which stem from the interaction of the eEDM with the internal magnetic field [5], second order terms arising from hyperfine corrections to the wave function have to be considered. As the operators $\hat{H}_{\text{d,I}}$ and $\hat{H}_{\text{d,II}}$ arise from a transformation of the Dirac-Coulomb Hamiltonian, magnetic terms emerging from this transformation would have to be considered as well (for a detailed discussion see, e.g., [22]).

Furthermore, additional magnetic contributions arise from the ZORA transformation due to the vector potential appearing on the off-diagonal elements of the Hamiltonian matrix.

Regarding many-body effects of the operator itself, things would become more complicated in a DFT picture, where only one-electron operators are well defined. Whereas the direct contribution could be calculated analogously to HF, a

correction term to the exchange-correlation potential would appear and special exchange-correlation energy functionals would have to be designed. In case of hybrid DFT, additionally Fock exchange contributions would have to be computed. Herein, however, an inclusion of such correction terms is not attempted.

In our present calculations all these many-electron operators are neglected. In principle, this could cause a deviation from comparable four-component calculations, which becomes in relative terms more pronounced in light molecules than in high-Z molecules and is expected to originate mainly from the terms (32) and (34). But these are still expected to be small.

This concludes our general discussion of many-electron effects in light molecules and we will present in the following the computational details of our numerical studies.

III. COMPUTATIONAL DETAILS

Quasirelativistic two-component calculations are performed within ZORA at the level of complex generalized Hartree-Fock (cGHF) or Kohn-Sham (cGKS) with a modified version [16,37–40] of the quantum chemistry program package Turbomole [41]. In order to calculate the $\mathcal{P},\mathcal{T}$-odd properties, the program was extended with the corresponding ZORA Hamiltonians (see [16] for details on the implementation).

For Kohn-Sham (KS)-density functional theory (DFT) calculations the hybrid Becke three parameter exchange functional and Lee, Yang, and Parr correlation functional (B3LYP) [42–45] was employed. In comparison to relativistic coupled cluster calculations this functional performed well for the description of $\mathcal{P},\mathcal{T}$-odd effects in diatomic radicals in our previous work, which motivates the present choice [16].

For all calculations a basis set of 37 s, 34 p, 14 d, and 9 f uncontracted Gaussian functions with the exponential coefficients α_i composed as an even-tempered series by $\alpha_i = ab^{N-i}; i = 1,\ldots,N$, with $b = 2$ for s and p function and with $b = (5/2)^{1/25} \times 10^{2/5} \approx 2.6$ for d and f functions was used for the electropositive atom (for details see the Supplemental Material [46]).[2] This basis set has proven successful in calculations of nuclear-spin dependent $\mathcal{P}$-violating interactions and $\mathcal{P},\mathcal{T}$-odd effects induced by an eEDM in heavy polar diatomic molecules [16,23,39,47]. The N, F, and O atoms were represented with a decontracted atomic natural orbital (ANO) basis set of triple-ζ quality [48] and for H the s,p subset of a decontracted correlation-consistent basis of quadruple-ζ quality [49] was used.

The ZORA-model potential $\tilde{V}(\vec{r})$ was employed with additional damping [50] as proposed by van Wüllen [25].

The model potential of O g, the element with highest Z of all known elements [51], was renormalized to the nuclear charge number of E120 and E121. These renormalized model potentials were employed in all calculations of molecules containing E120 and E121, respectively.

For calculations of two-component wave functions and properties a finite nucleus was used, described by a normalized spherical Gaussian nuclear density distribution $\rho_A(\vec{r}) = \frac{\zeta_A^{3/2}}{\pi^{3/2}} e^{-\zeta_A|\vec{r}-\vec{r}_A|^2}$. The mass numbers A were chosen as nearest integer to the standard relative atomic mass, i.e., ^{11}B, ^{24}Mg, ^{27}Al, ^{40}Ca, ^{45}Sc, ^{48}Ti, ^{65}Zn, ^{70}Ga, ^{88}Sr, ^{90}Y, ^{91}Zr, ^{112}Cd, ^{115}In, ^{137}Ba, ^{139}La, ^{140}Ce, ^{173}Yb, ^{175}Lu, ^{178}Hf, ^{201}Hg, ^{204}Tl, ^{226}Ra, ^{227}Ac, ^{232}Th, ^{259}No, ^{260}Lr, ^{261}Rf, ^{284}Cn; for E120 (unbinilium, Ubn, eka-actinium) and E121 (unbiunium, Ubu, eka-radium) the mass number was calculated by $2.5Z$, resulting in 300 and 303, respectively.

The nuclear equilibrium distances were obtained at the levels of GHF-ZORA and GKS-ZORA/B3LYP, respectively. As convergence criteria an energy change of less than $10^{-5}\ E_h$ was used. For DFT calculations of analytic energy gradients with respect to the displacement of the nuclei the nuclei were approximated as point charges. The equilibrium distances obtained are given in the Results section.

IV. RESULTS AND DISCUSSION

A. Numerical calculation of $\mathcal{P},\mathcal{T}$-violating properties

In this section the study of quite a number of diatomic molecules with $^2\Sigma_{1/2}$-ground state or for which at least a $^2\Sigma_{1/2}$-ground state can be expected, is presented. The set of molecules includes group 2 monofluorides (Mg–E120)F, group 3 mono-oxides (Sc–E121)O, group 4 mononitrides (Ti–Rf)N, group 12 monohydrides (Zn–Cn)H, group 13 monoxides (B–Tl)O, and the mononitrides (Ce–Th)N, monofluorides (Yb–No)F, and mono-oxides (Lu–Lr)O of some f-block groups, respectively.

The numerically calculated values of symmetry violating properties are presented for the listed molecules together with deviations between the methods cGHF and cGKS/B3LYP in Table I. The calculated equilibrium bond length r_e and numerical values of the reduced total electronic angular momentum projection quantum number Ω are shown as well.

The equilibrium bond lengths and values of Ω determined with GHF and GKS are typically in reasonable agreement. Large deviations in the bond length of about 0.1 a_0 are observed for LaO, YbF, and group 13 oxides excluding BO, indicating a more complicated electronic structure. Nearly all values of Ω are approximately equal to $\pm\frac{1}{2}$. Furthermore, in nearly all cases the reduced orbital angular momentum projection was $\Lambda \approx 0$ and thus there appears no significant contamination by Π states. Exceptions are CnH and RfN as well as TiN, which show large electron correlation effects (as gauged by the difference GHF-GKS) and seem to have a complicated electronic structure that requires more advanced electronic structure methods for a reliable description.

In the case of CnH the angular momentum projection quantum number was $\Omega = 0.5$, but some admixture of higher angular momentum states was found ($\Lambda \approx 0.14$). However, in the case of RfN and TiN $\Lambda \approx 0$ is valid and there was no significant admixture of Π contributions.

Especially in the case of RfN the methods employed herein are not able to give reliable results, indicated by enormous

[2]For the calculation of row 8 compounds the basis set was augmented with more diffuse functions and a set of g functions. However, these showed no remarkable influence on $\mathcal{P},\mathcal{T}$-odd properties and thus the results for the same basis set as for the other elements are presented.

TABLE I. Diatomic constants and $\mathcal{P},\mathcal{T}$-violating properties of diatomic molecules calculated *ab initio* within a quasirelativistic two-component ZORA approach at the cGHF and cGKS/B3LYP level. Dev. refers to the relative deviation $|\frac{W_{\mathrm{cGHF}}-W_{\mathrm{cGKS}}}{W_{\mathrm{cGHF}}}|$ between cGHF and cGKS results.

		r_e/a_0		Ω[a]		$W_s \frac{1}{h\,\mathrm{Hz}}$			$W_d \frac{e\,\mathrm{cm}}{10^{24}\,h\,\mathrm{Hz}}$		
Molecule	Z	cGHF	cGKS	cGHF	cGKS	cGHF	cGKS	Dev.	cGHF	cGKS	Dev.
						group 2 fluorides					
MgF	12	3:28	3:33	0.500	0.500	-5.93×10^{1}	-6.48×10^{1}	9%	-4.66×10^{-2}	-5.22×10^{-2}	12%
CaF	20	3.74	3.68	0.500	0.500	-2.19×10^{2}	-2.09×10^{2}	5%	-1.47×10^{-1}	-1.40×10^{-1}	4%
SrF	38	3.98	3.94	−0.500	0.500	-2.01×10^{3}	-1.94×10^{3}	4%	−1.05	−1.01	3%
BaF	56	4.16	4.11	0.500	0.500	-8.67×10^{3}	-7.58×10^{3}	13%	−3.32	−2.90	12%
RaF	88	4.30	4.26	−0.500	−0.500	-1.52×10^{5}	-1.36×10^{5}	10%	-2.80×10^{1}	-2.51×10^{1}	10%
E120F	120	4.37	4.36	0.500	0.499	-3.98×10^{6}	-3.45×10^{6}	13%	-3.49×10^{2}	-3.02×10^{2}	14%
						group 3 oxides					
ScO	21	3.15	3.14	0.500	0.500	-3.65×10^{2}	-2.83×10^{2}	22%	-2.42×10^{-1}	-1.87×10^{-1}	23%
YO	39	3.37	3.39	0.500	0.500	-3.04×10^{3}	-2.54×10^{3}	17%	−1.58	−1.32	17%
LaO	57	3.60	3.46	0.500	0.500	-1.30×10^{4}	-1.01×10^{4}	22%	−4.82	−3.76	22%
AcO	89	3.64	3.67	0.500	−0.500	-2.42×10^{5}	-1.94×10^{5}	20%	-4.34×10^{1}	-3.49×10^{1}	20%
E121O	121	3.82	3.87	−0.500	0.500	-7.41×10^{6}	-4.94×10^{6}	33%	-6.36×10^{2}	-4.24×10^{2}	33%
						group 4 nitrides					
TiN	22	2.94	2.94	0.358	0.358	-6.80×10^{2}	-3.18×10^{2}	53%	-4.37×10^{-1}	-2.06×10^{-1}	53%
ZrN	40	3.11	3.19	0.492	0.492	-3.96×10^{3}	-2.68×10^{3}	32%	−2.00	−1.37	32%
HfN	72	3.30	3.26	0.500	0.500	-1.09×10^{5}	-5.79×10^{4}	47%	-2.93×10^{1}	-1.58×10^{1}	46%
RfN[b]	104	3.55	3.48	(−0.500)	(−0.500)	(2.04×10^{6})	(1.60×10^{5})	92%	(2.51×10^{2})	(1.70×10^{1})	93%
						f-block nitrides					
CeN	58	3.29	3.26	0.500	0.500	-1.65×10^{4}	-1.18×10^{4}	28%	−5.94	−4.32	27%
ThN	90	3.41	3.44	0.500	0.500	-3.50×10^{5}	-2.64×10^{5}	25%	-6.10×10^{1}	-4.62×10^{1}	24%
						f-block uorides					
YbF	70	3.90	3.76	0.500	0.489	-4.12×10^{4}	-3.46×10^{4}	16%	-1.16×10^{1}	−9.69	16%
NoF	102	3.96	3.92	0.500	−0.500	-7.37×10^{5}	-7.38×10^{5}	0%	-9.65×10^{1}	-9.65×10^{1}	0%
						f-block oxides					
LuO	71	3.41	3.39	0.500	0.500	-6.57×10^{4}	-5.59×10^{4}	15%	-1.81×10^{1}	-1.55×10^{1}	15%
LrO	103	3.51	3.53	−0.500	−0.500	-1.22×10^{6}	-9.38×10^{5}	23%	-1.56×10^{2}	-1.21×10^{2}	23%
						group 12 hydrides					
ZnH	30	3.05	3.04	−0.500	−0.500	-2.03×10^{3}	-1.94×10^{3}	4%	−1.14	−1.09	4%
CdH	48	3.36	3.38	0.500	0.500	-1.51×10^{4}	-1.32×10^{4}	12%	−6.35	−5.59	12%
HgH	80	3.30	3.33	0.500	0.500	-3.77×10^{5}	-2.63×10^{5}	30%	-7.98×10^{1}	-5.60×10^{1}	30%
CnH	112	3.04	3.13	0.500	−0.500	-8.51×10^{6}	-5.26×10^{6}	38%	-8.69×10^{2}	-5.38×10^{2}	38%
						group 13 oxides					
BO	5	2.23	2.27	−0.500	−0.500	8.88	9.31	5%	9.42×10^{-3}	1.05×10^{-2}	12%
AlO	13	3.17	3.07	0.500	0.500	-5.59×10^{1}	-1.17×10^{2}	109%	-2.12×10^{-2}	-7.91×10^{-2}	272%
GaO	31	3.37	3.24	0.500	0.500	-1.45×10^{3}	-2.15×10^{3}	48%	-7.72×10^{-1}	−1.17	51%
InO	49	3.79	3.67	−0.500	−0.500	-9.25×10^{3}	-1.09×10^{4}	18%	−3.75	−4.45	19%
TlO	81	4.09	3.86	0.500	0.500	-2.35×10^{5}	-1.63×10^{5}	30%	-4.92×10^{1}	-3.42×10^{1}	31%

[a]The absolute sign of Ω is arbitrary. However, relative to the sign of the effective electric field $W_d\Omega$ it is always such that $\mathrm{sgn}(W_d) = -1$. Exceptions from this (RfN and BO) are discussed in the text.

[b]No reliable results could be obtained for RfN.

differences (by an order of magnitude in the case of the $\mathcal{P},\mathcal{T}$-odd parameters) between DFT and HF calculations, not only for properties but also for the ordering and pairing of molecular spin orbitals. The values given for RfN are only included for completeness, but are not to be considered as estimates of the expected effect sizes. Therefore, results for RfN are omitted in the plots presented below.

In Table II deviations between results obtained with the Hamiltonian in Eq. (7) and those computed with the Hamiltonian of Eq. (13) are shown for all molecules that are content of our paper (except RfN). This table shows that deviations between stratagem I and II are only in molecules containing super heavy elements noteworthy but remain always below 10% and thus are not important for the present discussion.

Furthermore, calculations with an internal electric field stemming from explicitly Gaussian shaped nuclei are compared to results of calculations with an internal electric field that stems from a pointlike nucleus in Table II.

TABLE II. Differences of $\mathcal{P},\mathcal{T}$-odd eEDM enhancement in diatomic molecules in a $^2\Sigma_{1/2}$-ground state between different forms of the interaction operator calculated *ab initio* within a quasirelativistic two-component ZORA approach at the cGHF and cGKS/B3LYP level. Relative difference $\Delta_{\mathrm{I/II}} = |\frac{W_{\mathrm{d,I}}-W_{\mathrm{d,II}}}{W_{\mathrm{d,II}}}|$ between strategem I [Eq. (7)] and II [Eq. (13)] and $\Delta_{\mathrm{IG/II}} = |\frac{W_{\mathrm{d,I,Gauß}}-W_{\mathrm{d,II}}}{W_{\mathrm{d,II}}}|$ between strategem I with internal electric field of a Gaussian shaped nucleus [Eq. (11)] and II [Eq. (13)].

		$W_{\mathrm{d}}^{\mathrm{cGHF}}\,\frac{e\,\mathrm{cm}}{10^{24}\,h\,\mathrm{Hz}}$					$W_{\mathrm{d}}^{\mathrm{cGKS}}\,\frac{e\,\mathrm{cm}}{10^{24}\,h\,\mathrm{Hz}}$				
Molecule	Z	$W_{\mathrm{d,I}}$	$W_{\mathrm{d,I,Gauß}}$	$W_{\mathrm{d,II}}$	$\Delta_{\mathrm{I/II}}$	$\Delta_{\mathrm{IG/II}}$	$W_{\mathrm{d,I}}$	$W_{\mathrm{d,I,Gauß}}$	$W_{\mathrm{d,II}}$	$\Delta_{\mathrm{I/II}}$	$\Delta_{\mathrm{IG/II}}$
				group 2 fluorides							
MgF	12	-4.66×10^{-2}	-4.69×10^{-2}	-4.56×10^{-2}	2%	3%	-5.22×10^{-2}	-5.26×10^{-2}	-5.12×10^{-2}	2%	3%
CaF	20	-1.47×10^{-1}	-1.48×10^{-1}	-1.44×10^{-1}	2%	2%	-1.40×10^{-1}	-1.41×10^{-1}	-1.38×10^{-1}	2%	2%
SrF	38	-1.05	-1.06	-1.04	1%	2%	-1.01	-1.02	-1.00	1%	2%
BaF	56	-3.32	-3.33	-3.28	1%	1%	-2.90	-2.91	-2.87	1%	1%
RaF	88	-2.80×10^{1}	-2.76×10^{1}	-2.73×10^{1}	3%	1%	-2.51×10^{1}	-2.47×10^{1}	-2.44×10^{1}	3%	1%
E120F	120	-3.49×10^{2}	-3.23×10^{2}	-3.20×10^{2}	8%	1%	-3.02×10^{2}	-2.79×10^{2}	-2.76×10^{2}	8%	1%
				group 3 oxides							
ScO	21	-2.42×10^{-1}	-2.44×10^{-1}	-2.38×10^{-1}	2%	2%	-1.87×10^{-1}	-1.89×10^{-1}	-1.84×10^{-1}	2%	2%
YO	39	-1.58	-1.59	-1.56	1%	2%	-1.32	-1.32	-1.30	1%	2%
LaO	57	-4.82	-4.83	-4.76	1%	1%	-3.76	-3.76	-3.71	1%	1%
AcO	89	-4.34×10^{1}	-4.27×10^{1}	-4.22×10^{1}	3%	1%	-3.49×10^{1}	-3.43×10^{1}	-3.39×10^{1}	3%	1%
E121O	121	-6.36×10^{2}	-5.86×10^{2}	-5.80×10^{2}	9%	1%	-4.24×10^{2}	-3.90×10^{2}	-3.87×10^{2}	9%	1%
				group 4 nitrides							
TiN	22	-4.37×10^{-1}	-4.40×10^{-1}	-4.30×10^{-1}	1%	2%	-2.06×10^{-1}	-2.08×10^{-1}	-2.03×10^{-1}	2%	2%
ZrN	40	-2.00	-2.01	-1.98	1%	2%	-1.37	-1.37	-1.35	1%	2%
HfN	72	-2.93×10^{1}	-2.92×10^{1}	-2.89×10^{1}	2%	1%	-1.58×10^{1}	-1.58×10^{1}	-1.56×10^{1}	2%	1%
				f-block nitrirides							
CeN	58	-5.94	-5.95	-5.87	1%	1%	-4.32	-4.33	-4.27	1%	1%
ThN	90	-6.10×10^{1}	-5.98×10^{1}	-5.92×10^{1}	3%	1%	-4.62×10^{1}	-4.53×10^{1}	-4.49×10^{1}	3%	1%
				f-block uorides							
YbF	70	-1.16×10^{1}	-1.15×10^{1}	-1.14×10^{1}	2%	1%	-9.69	-9.65	-9.55	1%	1%
NoF	102	-9.65×10^{1}	-9.32×10^{1}	-9.23×10^{1}	4%	1%	-9.65×10^{1}	-9.32×10^{1}	-9.22×10^{1}	4%	1%
				f-block oxides							
LuO	71	-1.81×10^{1}	-1.81×10^{1}	-1.79×10^{1}	2%	1%	-1.55×10^{1}	-1.54×10^{1}	-1.52×10^{1}	2%	1%
LrO	103	-1.56×10^{2}	-1.50×10^{2}	-1.49×10^{2}	5%	1%	-1.21×10^{2}	-1.16×10^{2}	-1.15×10^{2}	5%	1%
				group 12 hydrides							
ZnH	30	-1.14	-1.15	-1.13	1%	1%	-1.09	-1.10	-1.09	1%	1%
CdH	48	-6.35	-6.38	-6.30	1%	1%	-5.59	-5.61	-5.55	1%	1%
HgH	80	-7.98×10^{1}	-7.90×10^{1}	-7.83×10^{1}	2%	1%	-5.60×10^{1}	-5.54×10^{1}	-5.49×10^{1}	2%	1%
CnH	112	-8.69×10^{2}	-8.20×10^{2}	-8.13×10^{2}	6%	1%	-5.38×10^{2}	-5.08×10^{2}	-5.04×10^{2}	6%	1%
				group 13 oxides							
BO	5	9.42×10^{-3}	9.50×10^{-3}	9.19×10^{-3}	2%	3%	1.05×10^{-2}	1.06×10^{-2}	1.02×10^{-2}	3%	4%
AlO	13	-2.12×10^{-2}	-2.14×10^{-2}	-2.11×10^{-2}	1%	2%	-7.91×10^{-2}	-7.97×10^{-2}	-7.77×10^{-2}	2%	3%
GaO	31	-7.72×10^{-1}	-7.77×10^{-1}	-7.68×10^{-1}	1%	1%	-1.17	-1.18	-1.16	1%	1%
InO	49	-3.75	-3.76	-3.72	1%	1%	-4.45	-4.46	-4.41	1%	1%
TlO	81	-4.92×10^{1}	-4.87×10^{1}	-4.82×10^{1}	2%	1%	-3.42×10^{1}	-3.38×10^{1}	-3.35×10^{1}	2%	1%

A comparison with enhancement factors calculated with the internal electric field of a Gaussian nucleus shows that deviations between stratagem I and stratagem II in heavy nuclei stem solely from the finite size of the nucleus, which is implicitly included in the Hamiltonian of stratagem II. As expected, two-electron effects are larger than 1% for light elements only.

Returning again to the results obtained with the Hamiltonian of Eq. (7), we can observe large deviations between GHF and GKS values of W_{d} and W_{s} for some of the group 13 oxides (especially AlO and GaO). These indicate that there are electron correlation effects which cannot accurately be described by the present approaches. In these compounds also large spin-polarization effects could be observed. Especially for AlO more sophisticated electronic structure methods should be applied, if higher accuracy is desired. Nonetheless, for the present discussion of overall trends the description within the cGHF/cGKS scheme appears to suffice.

Generally the agreement between the HF and DFT descriptions is within 20% to 30%. Yet, in cases where d orbitals play an important role, such as group 4 nitrides or group 12 hydrides, additional electron correlation considered via the

DFT method has a pronounced impact on the value of the $\mathcal{P},\mathcal{T}$-odd properties. In case of mercury monofluoride these effects where already discussed in Ref. [16].

The two parameters W_d and W_s behave analogously with respect to inclusion of additional electron correlation effects when going along the periodic table.

The largest enhancement of $\mathcal{P},\mathcal{T}$-odd effects can be found in compounds of the seventh and eighth row of the periodic table, i.e., RaF, AcO, ThN, NoF, LrO, (RfN), CnH, E120F, and E121O. But also some compounds of the sixth row show enhancement of a similar of magnitude, namely HfN, HgH, TlO, YbF, and LuO. It shall be noted that even the exotic molecule CnH may be a candidate for future experiments, since ongoing research aims to achieve very long lived isotopes for the super heavy element Cn [52–54].

The investigation of $\mathcal{P},\mathcal{T}$-violation in group 13 oxides shows problems for the methods employed herein, as mentioned above. As comparatively large enhancement effects were calculated for TlO, a study of this molecule with more sophisticated electronic structure methods could be interesting in order to obtain an accurate description of its electronic structure. Little is known about TlO from the experimental side, however, so that significant further research would be necessary to take advantage of such enhancement effects.

B. Estimation of $\mathcal{P},\mathcal{T}$-violating properties from atomic scaling relations

In order to gain deeper insight into the scaling behavior of the above discussed properties the numerical results can be compared to analytical and empirical atomic models. Using the relations presented in the theory section [Eqs. (24) and (27)] within the quasirelativistic GHF/GKS-ZORA approach the parameter W_d is estimated from W_s and compared to the results of the numerical calculations.

Results for estimations of W_d from W_s for both the analytically derived expression by Sandars and the empirical factor found by Fermi and Segrè are shown in Table III, where again the labels FS and CS are used for properties calculated with the corresponding factors $\tilde{R}_{CS}$ and $\tilde{R}_{FS}$.

Relative deviations of the estimated $\mathcal{P},\mathcal{T}$-odd property W_d from the numerical calculations are typically below 10% for molecules with $Z < 100$. For light molecules of the first (BO) or second row (MgF, AlO) the deviations are much larger. In this region the atomic models do not work well. For these cases with light elements both the analytically derived CS equation and the empirical FS relation yield much too low (BO, AlO) or too high (MgF) values of W_d. It has to be pointed out that the case of BO is somewhat special, since boron is even lighter than oxygen and the "heavy" atom of this molecule is actually oxygen. By this also the sign of the $\mathcal{P},\mathcal{T}$-odd properties W_d and W_s is reversed and a different behavior than for all other group 13 compounds is expected.

In the region of super heavy elements ($Z > 100$) the abruptly rising analytically derived relativistic enhancement factor of the eEDM (reaching infinity at $Z \sim 118.65$) causes a large overestimation of W_d resulting in deviations of $\geqslant$35% for NoF ($Z = 102$) and LrO ($Z = 103$) and 146% for CnH ($Z = 112$) between the estimate and the numerical value. Here the empirical factor performs much better and a much lower increase in the deviation from the numerical calculations can be observed. However, even in the case of the empirically obtained relativistic enhancement factor the $\mathcal{P},\mathcal{T}$-odd enhancement in super heavy element compounds is strongly overestimated (deviations $\gg$10%) with these simple atomic models. This may be explained with the influence of the pole at $Z > 137$ of the used relativistic enhancement factors.

For the two studied compounds with $Z > 118$ the analytically derived factor is not applicable anymore, which results in deviations far beyond 500%, whereas the estimates obtained with the empirical factor deviate still less than 100% from numerical calculations. Nonetheless, the influence of the pole at $Z = 137$ of the relativistic enhancement factors for eEDM induced permanent molecular EDMs and scalar-pseudoscalar nucleon-electron current interactions causes deviations >10%.

C. Ratio of $\mathcal{P},\mathcal{T}$-violating properties

Various $\mathcal{P},\mathcal{T}$-odd parameters contribute to a permanent EDM in a molecule. In order to set limits on more than one parameter, experiments with different sensitivity to the $\mathcal{P},\mathcal{T}$-odd parameters have to be compared (for a detailed discussion see Refs. [55] or [56]).

In the following we numerically determine the trends of the ratio of $\mathcal{P},\mathcal{T}$-odd enhancement parameters in the periodic table and analyze how the sensitivity of an experiment to the herein discussed $\mathcal{P},\mathcal{T}$-odd effects d_e and k_s is influenced by the choice of the molecule.

As pointed out in Sec. II B, Dzuba *et al.* proposed an analytical model [Eq. (24)] for determination of the ratio W_d/W_s in atoms and diatomic molecules [35]. In their paper, however, its applicability was not generally tested for diatomic molecules, but only for the example of YbF. In the following we compare the analytical model of Ref. [35], with the improved version (27) and compare them to our numerical calculations.

The ratio W_d/W_s of the various open-shell diatomic molecules is studied, for which both the analytically derived and the empirically derived relativistic enhancement factors presented in Sec. II are compared. In Fig. 2 the ratio W_d/W_s calculated with the four different relativistic enhancement factors $\tilde{R}$ [Eqs. (24)–(28b)] is compared to all numerical results for the value of W_d/W_s. The empirically derived relativistic enhancement factor for W_d included in Eqs. (27) and (28b) is in much better agreement with the numerical results for $Z > 90$ as was also seen in the last section in the comparison of estimates of W_d with numerical values. Furthermore, values calculated with the improved relativistic enhancement factor for W_s [Eq. (22)] are in better agreement with numerical values also for $Z \ll 90$.

However, all the ratios derived from the analytical models show a wrong behavior in the region of $Z < 30$ and $Z > 90$ in comparison to the numerical results. This causes large deviations for the estimates discussed in the last section.

A logarithmic plot of the numerical results (see Fig. 3) shows an exponential behavior of the ratio of $\mathcal{P},\mathcal{T}$-odd properties W_d/W_s, which can be interpolated by a linear fit model

TABLE III. eEDM enhancement parmeter W_d of diatomic molecules estimated from numerically calculated $\mathcal{P},\mathcal{T}$-odd interaction parameter W_s via an analytical and an empirical relation from atomic considerations and comparison to numerical results. $\Delta_{CS/FS} = |\frac{W_d - W_{d,CS/FS}}{W_d}|$ refers to the relative deviation of estimates with respect to numerical calculations.

		cGHF				cGKS			
Molecule	Z	$W_{d,CS}\,\frac{e\,cm}{10^{24}\times h\,Hz}$	Δ_{CS}	$W_{d,FS}\,\frac{e\,cm}{10^{24}\times h\,Hz}$	Δ_{FS}	$W_{d,CS}\,\frac{e\,cm}{10^{24}\times h\,Hz}$	Δ_{CS}	$W_{d,FS}\,\frac{e\,cm}{10^{24}\times h\,Hz}$	Δ_{FS}
				group 2 fluorides					
MgF	12	-4.2×10^{-2}	11%	-4.2×10^{-2}	11%	-4.5×10^{-2}	13%	-4.5×10^{-2}	13%
CaF	20	-1.4×10^{-1}	3%	-1.4×10^{-1}	2%	-1.4×10^{-1}	3%	-1.4×10^{-1}	3%
SrF	38	-1.0	1%	-1.0	0%	-10.0×10^{-1}	2%	-1.0	0%
BaF	56	-3.2	3%	-3.3	0%	-2.8	3%	-2.9	0%
RaF	88	-3.0×10^{1}	8%	-3.0×10^{1}	8%	-2.7×10^{1}	8%	-2.7×10^{1}	8%
E120F	120	-3.1×10^{3}	981%	-6.1×10^{2}	75%	-2.7×10^{3}	983%	-5.3×10^{2}	76%
				group 3 oxides					
ScO	21	-2.4×10^{-1}	2%	-2.4×10^{-1}	2%	-1.8×10^{-1}	2%	-1.8×10^{-1}	2%
YO	39	-1.5	3%	-1.6	1%	-1.3	3%	-1.3	1%
LaO	57	-4.7	2%	-4.8	1%	-3.7	2%	-3.8	1%
AcO	89	-4.8×10^{1}	9%	-4.7×10^{1}	9%	-3.8×10^{1}	9%	-3.8×10^{1}	9%
E121O	121	-3.1×10^{3}	582%	-1.2×10^{3}	84%	-2.0×10^{3}	582%	-7.8×10^{2}	84%
				group 4 nitrides					
TiN	22	-4.4×10^{-1}	0%	-4.4×10^{-1}	0%	-2.0×10^{-1}	1%	-2.0×10^{-1}	1%
ZrN	40	-2.0	2%	-2.0	0%	-1.3	2%	-1.4	1%
HfN	72	-2.9×10^{1}	1%	-3.0×10^{1}	3%	-1.6×10^{1}	1%	-1.6×10^{1}	1%
RfN[a]	104	(3.7×10^{2})	47%	(3.1×10^{2})	23%	(2.9×10^{1})	70%	(2.4×10^{1})	43%
				f-block nitrides					
CeN	58	-5.9	1%	-6.0	2%	-4.2	2%	-4.3	0%
ThN	90	-6.8×10^{1}	11%	-6.7×10^{1}	10%	-5.1×10^{1}	11%	-5.1×10^{1}	10%
				f-block uorides					
YbF	70	-1.2×10^{1}	0%	-1.2×10^{1}	3%	-9.7	0%	-10.0	3%
NoF	102	-1.3×10^{2}	35%	-1.1×10^{2}	19%	-1.3×10^{2}	36%	-1.1×10^{2}	19%
				f-block oxides					
LuO	71	-1.8×10^{1}	0%	-1.9×10^{1}	2%	-1.5×10^{1}	1%	-1.6×10^{1}	2%
LrO	103	-2.2×10^{2}	39%	-1.9×10^{2}	20%	-1.7×10^{2}	39%	-1.4×10^{2}	20%
				group 12 hydrides					
ZnH	30	-1.2	3%	-1.2	4%	-1.1	3%	-1.1	4%
CdH	48	-6.5	3%	-6.7	5%	-5.7	2%	-5.8	4%
HgH	80	-8.7×10^{1}	9%	-8.8×10^{1}	11%	-6.0×10^{1}	8%	-6.2×10^{1}	10%
CnH	112	-2.1×10^{3}	146%	-1.2×10^{3}	41%	-1.3×10^{3}	146%	-7.6×10^{2}	40%
				group 13 oxides					
BO	5	6.5×10^{-3}	31%	6.5×10^{-3}	31%	6.8×10^{-3}	36%	6.8×10^{-3}	36%
AlO	13	-3.9×10^{-2}	83%	-3.9×10^{-2}	83%	-8.1×10^{-2}	3%	-8.1×10^{-2}	3%
GaO	31	-8.3×10^{-1}	8%	-8.4×10^{-1}	9%	-1.2	5%	-1.2	6%
InO	49	-3.9	5%	-4.0	7%	-4.6	4%	-4.7	6%
TlO	81	-5.3×10^{1}	8%	-5.4×10^{1}	9%	-3.7×10^{1}	8%	-3.8×10^{1}	10%

[a] No reliable results could be obtained for RfN.

with

$$\log_{10}\left\{\left|\frac{W_d}{W_s}\right|\times10^{-21}\,e\,cm\right\} = qZ + p. \tag{36}$$

In this plot Fig. 3 also results in calculations reported by Fleig for the two molecules HfF^+ and ThO, where a $^3\Delta$ state is of relevance for experiments, are included [57]. It can be inferred that the ratio W_d/W_s is rather insensitive to the chemical environment of the heavy nucleus, but is essentially determined by the exponential Z dependence determined in Fig. 3.

In order to disentangle the $\mathcal{P},\mathcal{T}$-odd parameters k_s and d_e, at least two experiments with molecules 1 and 2 are needed. The measurement model then is a 2×2-matrix problem described by the system of equations

$$h\begin{pmatrix}\nu_1\\ \nu_2\end{pmatrix} = \Omega\underbrace{\begin{pmatrix}W_{d,1} & W_{s,1}\\ W_{d,2} & W_{s,2}\end{pmatrix}}_{\mathbf{C}}\begin{pmatrix}d_e\\ k_s\end{pmatrix}, \tag{37}$$

where $\mathbf{C}$ is the matrix of sensitivity coefficients. We follow now Ref. [58] in order to describe the uncertainties and

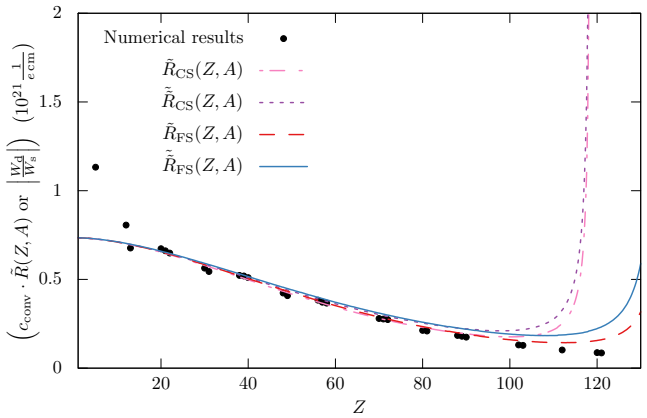

FIG. 2. Comparison of combined relativistic enhancement factors and conversion factors for the ratio between $\mathcal{P},\mathcal{T}$-odd eEDM and nucleon-electron current interactions $W_{\rm d}/W_{\rm s}$. The relativistic factors $\tilde{R}$ derived from the analytically derived factor (CS) and the empirical factor (FS) are shown, as well as their analogs derived from an old relativistic enhancement factor for $W_{\rm s}$ $\tilde{\tilde{R}}$. Plots are shown for the case of $j=\frac{1}{2}$ as in $^2\Sigma_{1/2}$ states. Mass numbers A were assumed as the natural mass number corresponding to the next integer value of Z. Numerical values shown are from cGKS calculations.

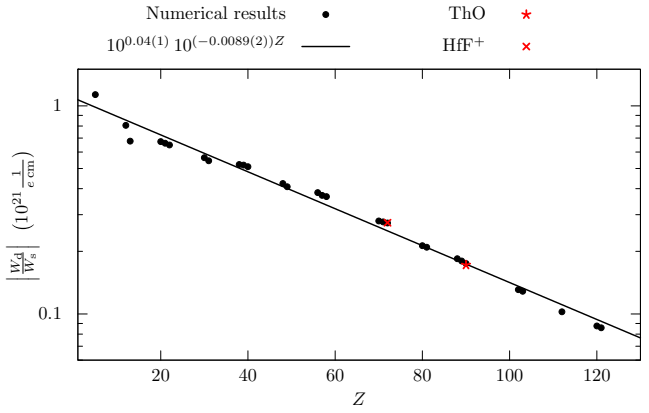

FIG. 3. Fit of the Z dependence of the ratio between $\mathcal{P},\mathcal{T}$-odd eEDM and scalar-pseudoscalar nucleon-electron current interactions $W_{\rm d}/W_{\rm s}$. The values of $W_{\rm d}/W_{\rm s}$ for HfF^+ and ThO were calculated by Fleig in a four-component configuration interaction framework in Ref. [57] and are shown for comparison but are not included in the fit. All other numerical values correspond to results from cGKS calculations.

coverage regions determined by two experiments. The covariance matrix $\mathbf{U}_{\mathcal{P},\mathcal{T}}$ of $k_{\rm s}$ and $d_{\rm e}$ can be obtained from the covariances of the measured frequencies $\mathbf{U}_\nu$ via the matrix product $\mathbf{C}^{-1}\mathbf{U}_\nu(\mathbf{C}^{-1})^T$. Assuming the measurements are uncorrelated, $\mathbf{U}_\nu$ is a diagonal matrix with the squared standard uncertainties of the measurements $u^2(\nu_1)$ and $u^2(\nu_2)$ on the diagonal. Thus the covariance matrix $\mathbf{U}_{\mathcal{P},\mathcal{T}}$ has the form

$$\mathbf{U}_{\mathcal{P},\mathcal{T}}=h^2\begin{pmatrix}\frac{u^2(\nu_1)}{\left(\frac{W_{\rm d,1}}{W_{\rm s,1}}-\frac{W_{\rm d,2}}{W_{\rm s,2}}\right)^2W_{\rm s,1}^2}+\frac{u^2(\nu_2)}{\left(\frac{W_{\rm d,1}}{W_{\rm s,1}}-\frac{W_{\rm d,2}}{W_{\rm s,2}}\right)^2W_{\rm s,2}^2} & -\frac{u^2(\nu_1)}{\frac{W_{\rm d,2}}{W_{\rm s,2}}\left(\frac{W_{\rm s,1}}{W_{\rm d,1}}-\frac{W_{\rm s,2}}{W_{\rm d,2}}\right)^2W_{\rm d,1}^2}-\frac{u^2(\nu_2)}{\frac{W_{\rm d,1}}{W_{\rm s,1}}\left(\frac{W_{\rm s,1}}{W_{\rm d,1}}-\frac{W_{\rm s,2}}{W_{\rm d,2}}\right)^2W_{\rm d,2}^2}\\ -\frac{u^2(\nu_1)}{\frac{W_{\rm d,2}}{W_{\rm s,2}}\left(\frac{W_{\rm s,1}}{W_{\rm d,1}}-\frac{W_{\rm s,2}}{W_{\rm d,2}}\right)^2W_{\rm d,1}^2}-\frac{u^2(\nu_2)}{\frac{W_{\rm d,1}}{W_{\rm s,1}}\left(\frac{W_{\rm s,1}}{W_{\rm d,1}}-\frac{W_{\rm s,2}}{W_{\rm d,2}}\right)^2W_{\rm d,2}^2} & \frac{u^2(\nu_1)}{\left(\frac{W_{\rm s,1}}{W_{\rm d,1}}-\frac{W_{\rm s,2}}{W_{\rm d,2}}\right)^2W_{\rm d,1}^2}+\frac{u^2(\nu_2)}{\left(\frac{W_{\rm s,1}}{W_{\rm d,1}}-\frac{W_{\rm s,2}}{W_{\rm d,2}}\right)^2W_{\rm d,2}^2}\end{pmatrix},\tag{38}$$

where we have expressed the sensitivity factors in terms of the $\mathcal{P},\mathcal{T}$-odd ratios. In order to set tight bounds on both of the $\mathcal{P},\mathcal{T}$-odd parameters the coverage region in the parameter space of $k_{\rm s}$ and $d_{\rm e}$ has to become small. We consider now the commonly applied case of an ellipsoidal coverage region. The $\mathcal{P},\mathcal{T}$-odd parameters are characterized by a bivariate Gaussian probability distribution function with $\binom{d_{\rm e}}{k_{\rm s}}$ and $\mathbf{U}_{\mathcal{P},\mathcal{T}}$. The ellipse centered at $\binom{d_{\rm e}}{k_{\rm s}}=\vec{0}$ is described by

$$\underbrace{\begin{pmatrix}x_{\rm d}\\x_{\rm s}\end{pmatrix}^T\mathbf{U}_{\mathcal{P},\mathcal{T}}^{-1}\begin{pmatrix}x_{\rm d}\\x_{\rm s}\end{pmatrix}}_{f_{\rm e}(x_{\rm d},x_{\rm s})}=k_p^2,\tag{39}$$

where $k_p=2.45$ for an elliptical region of 95% probability and $x_{\rm d}$ and $x_{\rm s}$ are the coordinates in the parameter space in direction of $d_{\rm e}$ and $k_{\rm s}$, respectively. Calculation of the inverse and the products yields an ellipse centered at $\binom{d_{\rm e}}{k_{\rm s}}=\vec{0}$ described by

$$f_{\rm e}(x_{\rm d},x_{\rm s})=\left(\frac{W_{\rm d,1}^2}{u^2(\nu_1)}+\frac{W_{\rm d,2}^2}{u^2(\nu_2)}\right)x_{\rm d}^2+2\left(\frac{W_{\rm d,1}^2}{u^2(\nu_1)}\frac{W_{\rm s,1}}{W_{\rm d,1}}+\frac{W_{\rm d,2}^2}{u^2(\nu_2)}\frac{W_{\rm s,2}}{W_{\rm d,2}}\right)x_{\rm d}x_{\rm s}+\left[\frac{W_{\rm d,1}^2}{u^2(\nu_1)}\left(\frac{W_{\rm s,1}}{W_{\rm d,1}}\right)^2+\frac{W_{\rm d,2}^2}{u^2(\nu_2)}\left(\frac{W_{\rm s,2}}{W_{\rm d,2}}\right)^2\right]x_{\rm s}^2.\tag{40}$$

The area of the ellipse can be readily evaluated via

$$A_{\rm ellipse}=\frac{2h^2k_p^2\pi}{\sqrt{\frac{\partial^2f_{\rm e}(x_{\rm d},x_{\rm s})}{\partial x_{\rm s}^2}\frac{\partial^2f_{\rm e}(x_{\rm d},x_{\rm s})}{\partial x_{\rm d}^2}-\left(\frac{\partial^2f_{\rm e}(x_{\rm d},x_{\rm s})}{\partial x_{\rm d}\partial x_{\rm s}}\right)^2}}.\tag{41}$$

Thus the ellipse has an area of

$$A_{\rm ellipse}=\frac{h^2k_p^2\pi\,|u(\nu_1)u(\nu_2)|}{|W_{\rm d,1}W_{\rm d,2}|\left|\frac{W_{\rm s,1}}{W_{\rm d,1}}-\frac{W_{\rm s,2}}{W_{\rm d,2}}\right|}.\tag{42}$$

In order to disentangle $d_{\rm e}$ and $k_{\rm s}$ in two experiments (1 and 2) and set tight limits, assuming equal uncertainties for experiments 1 and 2 the expression

$$|W_{\rm d,1}W_{\rm d,2}|\,0.91(2)|1.0207(5)^{Z_1}-1.0207(5)^{Z_2}|\times10^{-21}\,e\,\rm cm.\tag{43}$$

has to become large. The enhancement of the eEDM in both experiments, which is determined by $W_{\rm d,1}W_{\rm d,2}$ is strongly

dependent on the chemical environment, as will be discussed in the following sections. However, assuming at this point a scaling behavior of $W_{d,1}$ as in Eqs. (19) and (20) for atomic systems, the area of the coverage region is inversely proportional to

$$\frac{(Z_1 Z_2)^3}{\gamma_1^4 \gamma_2^4} 0.91(2)|1.0207(5)^{Z_1} - 1.0207(5)^{Z_2}| \times 10^{-21} \frac{1}{e\,\mathrm{cm}}. \tag{44}$$

Thus, in order to set tight limits on both $\mathcal{P},\mathcal{T}$-odd parameters, experiments with molecules that have a high nuclear charge and at the same time differ considerably in the nuclear charge Z of the electropositive atom are required. For example, when assuming equal uncertainties $u(\nu_i)$, a comparison of experiments with YbF and RaF or ThO would provide tighter bounds than a comparison of a BaF experiment with a ThO experiment but also than a comparison of experiments with RaF and ThO. However, the possibilities are limited for paramagnetic molecules because enhancement effects of the individual properties still increase steeply with increasing Z, which is the dominating effect. Alternatively experiments with diamagnetic atoms and molecules can further tighten bounds on d_e and k_s, as they show different dependencies on the nuclear charge (see, e.g., Refs. [55,59]).

This scheme can also be expanded for experiments that aim to set accurate limits on more than the herein discussed parameters. However, for this purpose first the respective enhancement factors have to be calculated for a systematic set of molecules. Furthermore, it should be noted that the present picture is not complete because of other sources of permanent EDMs that were not accounted for, namely $\mathcal{P},\mathcal{T}$-odd tensor and pseudoscalar-scalar electron-nucleon current interactions, as well as $\mathcal{P},\mathcal{T}$-odd nuclear dipole moments, which lead to the nuclear Schiff moment and nuclear magnetic quadrupole interactions (see for an overview, e.g., [3]).

D. Periodic trends of $\mathcal{P},\mathcal{T}$-violating properties

The analytical scaling relations presented in Eqs. (22), (19), and (20) can also be used to determine the numerical Z scaling within a group of compounds with electropositive atoms of the same column of the periodic table. For this purpose the property is divided by its relativistic enhancement factor and plotted on a logarithmic scale on both axes, as has been done for the nuclear spin-dependent $\mathcal{P}$-violating interaction parameter in Refs. [39,47,60]:

$$\log_{10}\left\{\frac{|W_s|}{R(Z,A)f(Z)^{\frac{\gamma+1}{2}}} \times \frac{1}{h\mathrm{Hz}}\right\} = b_s + \log_{10}\{Z^{a_s}\}, \tag{45}$$

$$\log_{10}\left\{|W_d|\gamma(4\gamma^2-1) \times 10^{-24}\frac{e\,\mathrm{cm}}{h\mathrm{Hz}}\right\} = b_{d,CS} + \log_{10}\{Z^{a_{d,CS}}\}, \tag{46}$$

$$\log_{10}\left\{|W_d|\gamma^4 \times 10^{-24}\frac{e\,\mathrm{cm}}{h\mathrm{Hz}}\right\} = b_{d,FS} + \log_{10}\{Z^{a_{d,FS}}\}. \tag{47}$$

From Eqs. (18) and (19) the exponents of Z can be expected to be approximately three. For both parameters the Z scaling is studied herein not only within columns, but also for isolobal diatomics within rows of the periodic table.

The resulting Z-scaling parameters a and Z-independent factors 10^b will be discussed in the following for both, GHF and GKS results.

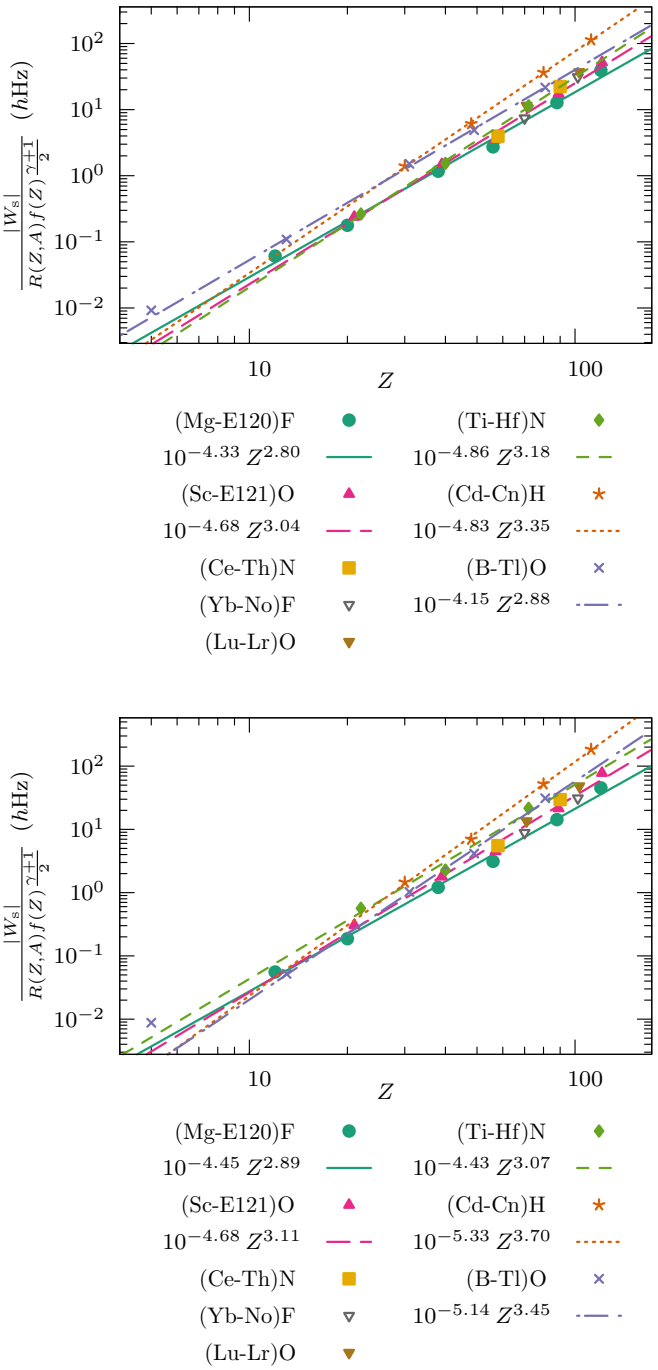

FIG. 4. Scaling of $\log_{10}\{\frac{|W_s|}{R(Z,A)f(Z)^{\frac{\gamma+1}{2}}} \times \frac{1}{h\mathrm{Hz}}\}$ with $\log_{10}\{Z\}$ for group 2 fluorides (Mg-E120)F, group 3 oxides (Sc-E121)O, group 4 nitrides (Ti-Hf)N, group 12 hydrides (Zn-Cn)H, and group 13 oxides (B-Tl)O at the level of GKS-ZORA/B3LYP (top) and GHF-ZORA (bottom). Corresponding functional expressions of the fits are plotted in each panel as a solid line, long-dashed line, short-dashed line, dotted line, and dash-dotted line, respectively. Plot of the f-block groups (Ce-Th)N, (Yb-No)F, and (Lu-Lr)O without fit. Boron was not included in the fit of group 13 oxides (see text).

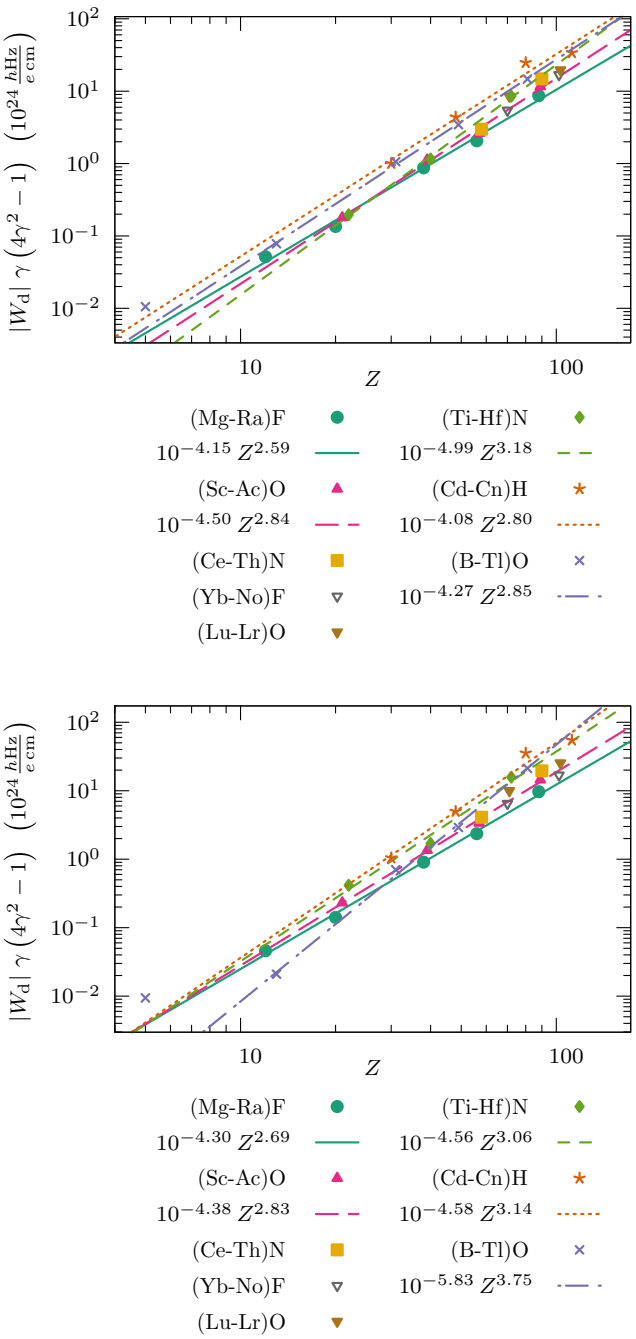

FIG. 5. Scaling of $\log_{10}\{|W_d|\gamma(4\gamma^2-1)\times 10^{-24}\,\frac{e\,\mathrm{cm}}{h\mathrm{Hz}}\}$ with $\log_{10}\{Z\}$ for group 2 fluorides (Mg-Ra)F, group 3 oxides (Sc-Ac)O, group 4 nitrides (Ti-Hf)N, group 12 hydrides (Zn-Cn)H, and group 13 oxides (B-Tl)O at the level of GKS-ZORA/B3LYP (top) and GHF-ZORA (bottom). Corresponding functional expressions of the fits are plotted in each panel as a solid line, long-dashed line, short-dashed line, dotted line, and dash-dotted line, respectively. Plot of the f-block groups (Ce-Th)N, (Yb-No)F, and (Lu-Lr)O without fit. Boron was not included in the fit of group 13 oxides (see text).

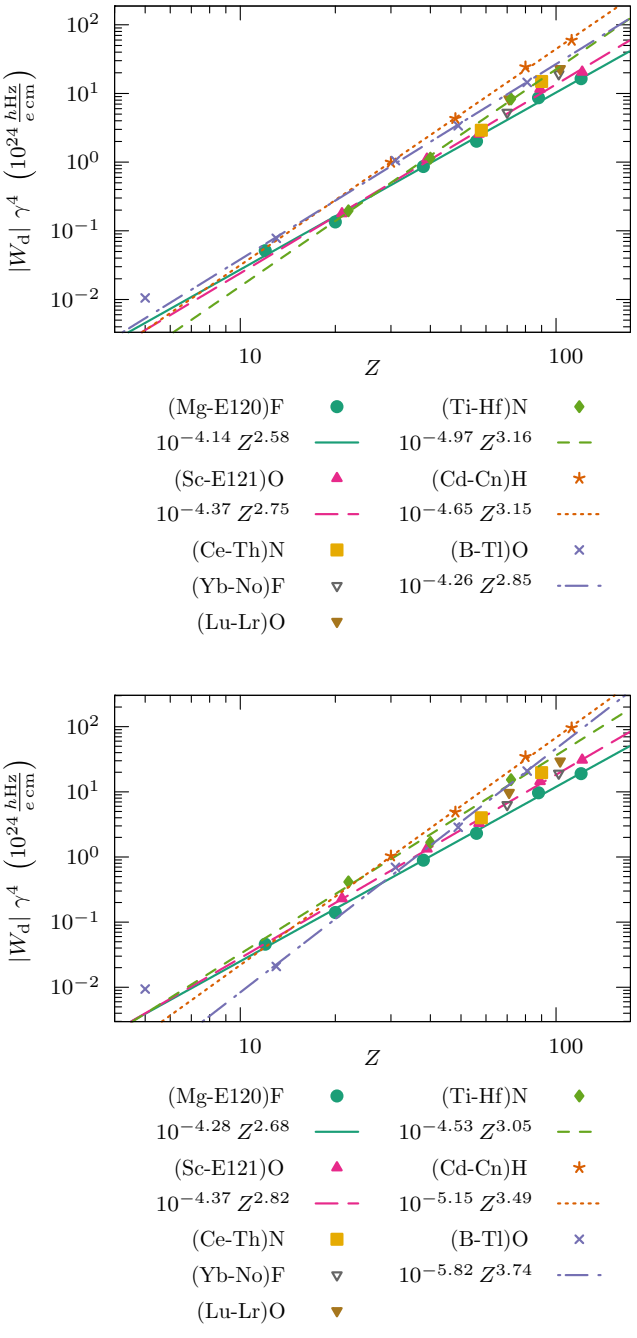

FIG. 6. Scaling of $\log_{10}\{|W_d|\gamma^4\times 10^{-24}\,\frac{e\,\mathrm{cm}}{h\mathrm{Hz}}\}$ with $\log_{10}\{Z\}$ for group 2 fluorides (Mg-E120)F, group 3 oxides (Sc-E121)O, group 4 nitrides (Ti-Hf)N, group 12 hydrides (Zn-Cn)H, and group 13 oxides (B-Tl)O at the level of GKS-ZORA/B3LYP (top) and GHF-ZORA (bottom). Corresponding functional expressions of the fits are plotted in each panel as a solid line, long-dashed line, short-dashed line, dotted line, and dash-dotted line, respectively. Plot of the f-block groups (Ce-Th)N, (Yb-No)F, and (Lu-Lr)O without fit. Boron was not included in the fit of group 13 oxides (see text).

1. Z scaling within groups of the periodic table

In the following the scaling within the groups of the periodic table is studied. The graphical representation of the Z scaling of W_s and W_d can be found in Figs. 4–6. In case of group 13 oxides, boron was not included in the linear fit, because it has a very different character (see discussion above).

Comparing the two different relativistic enhancement factors for eEDM interactions, which were employed in this study, we see for most of the groups of molecules no

TABLE IV. Z-scaling a and Z-independent factors b of $\frac{|W_s|}{R(Z,A)f(Z)\frac{\gamma+1}{2}}$ and $|W_d|\gamma^4$ (empirical relativistic enhancement factor) for group 2 fluorides (Mg-Ra)F, group 3 oxides (Sc-Ac)O, group 4 nitrides (Ti-Hf)N, group 12 hydrides (Zn-Cn)H, and group 13 oxides (Al-Tl)O at the level of GHF-ZORA and GKS-ZORA/B3LYP. Standard uncertainties of the fit are given in parentheses with respect to the last or two last significant digits.

	a_s		b_s		$a_{d,FS}$		$b_{d,FS}$	
Group	GHF	GKS	GHF	GKS	GHF	GKS	GHF	GKS
(Mg-E120)F	2.89(10)	2.80(12)	−4.45(17)	−4.33(19)	2.68(6)	2.58(8)	−4.28(10)	−4.14(14)
(Sc-E121)O	3.11(17)	3.04(13)	−4.7(3)	−4.7(2)	2.82(7)	2.75(11)	−4.37(12)	−4.37(19)
(Ti-Hf)N	3.1(4)	3.18(13)	−4.4(7)	−4.9(2)	3.0(4)	3.16(12)	−4.5(7)	−5.0(2)
(Cd-Cn)H	3.70(9)	3.35(5)	−5.33(17)	−4.83(10)	3.49(9)	3.15(9)	−5.15(18)	−4.65(16)
(Al-Tl)O	3.45(11)	2.88(6)	−5.14(17)	−4.15(10)	3.74(12)	2.85(6)	−5.82(19)	−4.26(9)

appreciable differences between the analytically derived and the empirical factor. Yet, in case of group 12 hydrides it is important to use the empirical scaling factor. Cn has a nuclear charge of $Z = 112$, which is close to the singularity of the analytically derived factor. This results in a strong overestimation of the relativistic enhancement and thus a strong underestimation of the plotted value, which explains the large deviations from a power relationship for group 12 hydrides in Fig. 5. Furthermore, with the analytically derived enhancement factor no meaningful plot that includes the row 8 compounds E120F and E121O is possible. Therefore, in the following we will use the results obtained with the empirical enhancement factor for our discussions.

The Z-scaling parameters a and the Z-independent prefactors 10^b are summarized in Table IV. It should be noted that the inclusion of the values of the row 8 compounds into the fit causes no notable changes in the Z scaling in case of the eEDM and $\mathcal{P},\mathcal{T}$-odd nucleon-electron current enhancement.

For all parameters the agreement between GHF and GKS calculations is excellent for group 2 fluorides, group 3 oxides, and group 4 nitrides, whereas DFT predicts a considerably different behavior for group 12 hydrides and group 13 oxides. As could be seen in [16] the DFT approach performs much better in the case of group 12 compounds than GHF due to pronounced electron correlation effects and therefore can be taken as more reliable. In the previous sections large electron correlation effects in group 13 compounds, which lead to large differences between GHF an GKS, were already discussed.

The scaling of $\mathcal{P},\mathcal{T}$-odd interactions seems to follow the same laws as that of nuclear spin-dependent $\mathcal{P}$-violating interactions studied in [39,60]. The Z scaling increases up to group 12 hydrides, when going along the periods of the periodic table. This maximum effect of $\mathcal{P},\mathcal{T}$-violation enhancement in group 12 compounds seen here is similar to the maximum of relativistic and quantum electrodynamic effects in group 11 compounds [61,62]. At the same time the Z-independent factor 10^b is smallest for these compounds. This damping is, however, only dominant in the region of small Z, which coincides with the findings in [39,60] for $\mathcal{P}$-odd interactions.

In [60] the large Z-scaling of group 4 and group 12 compounds compared to group 2 or 3 compounds was attributed mainly to the filling of the d shells, which causes an increment of the effective nuclear charge because the shielding of the nuclear charge by d orbitals is less efficient than by s or p orbitals. Furthermore, therein it was argued that the lower electronegativity of nitrogen compared to oxygen (group 4 shows larger scaling than group 3, although isoelectronic) causes the large effects in group 4 nitrides. A comparison of the molecules with f-block elements next to group 3, that is CeN and ThN, shows a similar behavior as for group 3 or group 2 compounds. Thus the filling of the f shell has a considerable effect on the size of $\mathcal{P},\mathcal{T}$-violating effects as well, which causes group 4 nitrides to be behave differently than group 3 oxides, whereas CeN and ThN are more similar to group 3 oxides.

Relating the Z scaling of the fits to the expected Z scaling [see Eqs. (18) and (19)], yields a quantitative Z-dependent factor for the effects of the molecular electronic structure on $\mathcal{P},\mathcal{T}$ violation. Referring to the GKS result we get an additional scaling factor of $\sim Z^{-0.2}$ for W_s and $\sim Z^{-0.4}$ for W_d for group 2 fluorides, thus there is some damping of $\mathcal{P},\mathcal{T}$-violating effects due to the electronic structure. This can be observed for group 3 oxides regarding eEDM enhancement as well ($Z^{-0.2}$ for W_d), but for W_s, in contrast, there is no additional Z-dependent damping.

A similar damping can be observed for group 13 oxides on the GKS level, whereas GHF predicts a considerable Z-dependent enhancement instead. The group 4 and 12 compounds show an additional Z-dependent enhancement of $\mathcal{P},\mathcal{T}$-odd effects: $\sim Z^{0.1}$ for W_s and W_d in group 4, $\sim Z^{0.4}$ for W_s, and $\sim Z^{0.2}$ for W_d in group 12. Thus we see a strong enhancement due to Z-dependent electronic structure effects in group 12 hydrides, which does not originate from relativistic enhancement factors obtained from atomic considerations based on Eqs. (18) and (19).

The Z-independent electronic structure factors 10^b show a behavior inverse to that of Z^a and are largest for group 2 fluorides and group 13 oxides in the DFT case, whereas the factors for group 12 hydrides and group 4 nitrides are almost an order of magnitude smaller. Yet, in GHF calculations the Z-independent effects are on the same order for group 13 oxides as for group 12 hydrides.

Now we can return to the discussion of disentanglement of d_e and k_s in the two-dimensional parameter space (Sec. IV C). With the chemical group specific effective Z dependence of the eEDM enhancement factors for paramagnetic molecules, Eq. (42) for the area in the parameter space of d_e and k_s covered by experiments with two different molecules 1 and 2

can be rewritten as

$$A_{\text{ellipse}} = \frac{k_p^2 \pi}{0.91(2) \times 10^{27} \frac{\text{Hz}^2}{e\,\text{cm}}} \times \frac{|u(v_1)u(v_2)|}{10^{b_{\text{d},1}+b_{\text{d},2}} \frac{Z_1^{a_{\text{d},1}} Z_2^{a_{\text{d},2}}}{\gamma_1^4 \gamma_2^4} |1.0207(5)^{Z_1} - 1.0207(5)^{Z_2}|}. \quad (48)$$

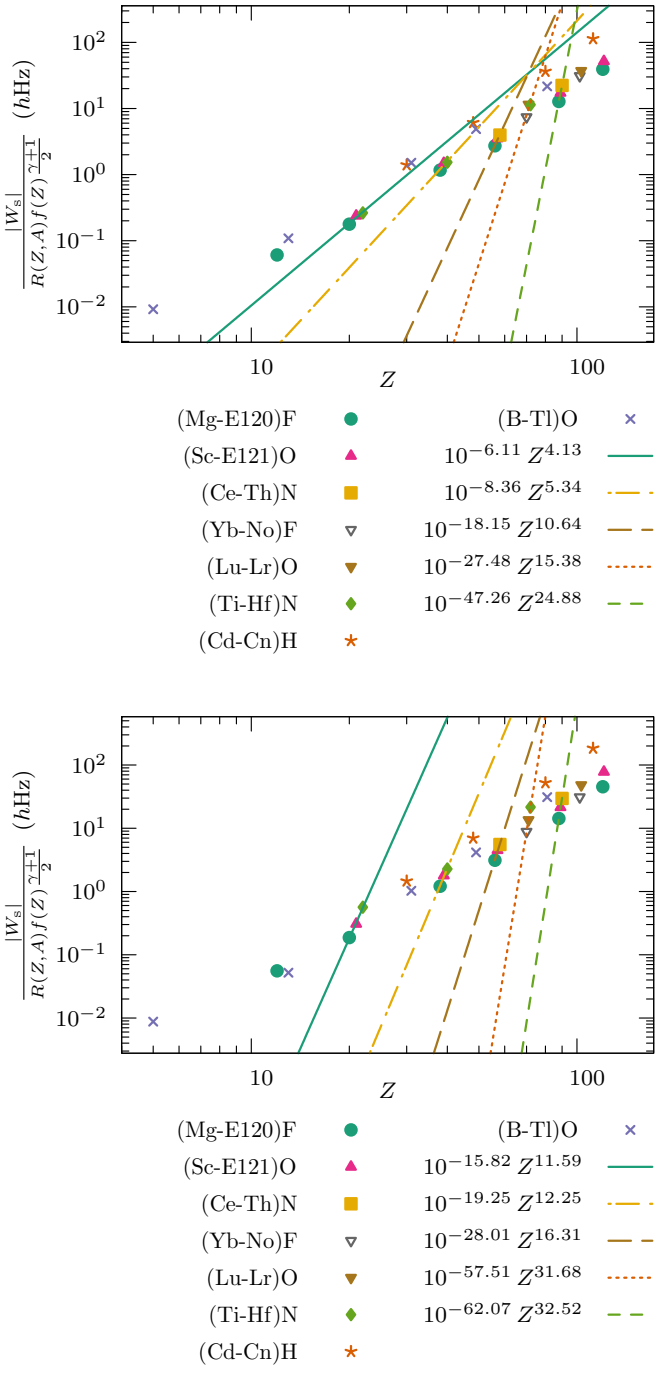

FIG. 7. Scaling of $\log_{10}\{\frac{|W_s|}{R(Z,A)f(Z)^{\frac{\gamma+1}{2}}} \times \frac{1}{h\text{Hz}}\}$ with $\log_{10}\{Z\}$ for row 4 (Ca-Ti; solid line), row 5 (Sr-Zr; dash-dotted line), row 6 (Ba-Ce; long-dashed line, Yb-Hf; dotted line), and row 7 (Ra-Th; short-dashed line) at the level of GKS-ZORA/B3LYP (top) and GHF-ZORA (bottom).

Here the factor 10^{27} and the units result from Eq. (47), wherein W_d is in units of $10^{24}\,\frac{h\text{Hz}}{e\,\text{cm}}$.

What remains to be analyzed in future works is the detailed influence of molecular orbitals on $\mathcal{P}, \mathcal{T}$-violating effects that causes the observed enhancement effects.

2. Z scaling of isolobal molecules

Now we focus on the Z scaling for isolobal diatomic molecules within the rows of the periodic table. When

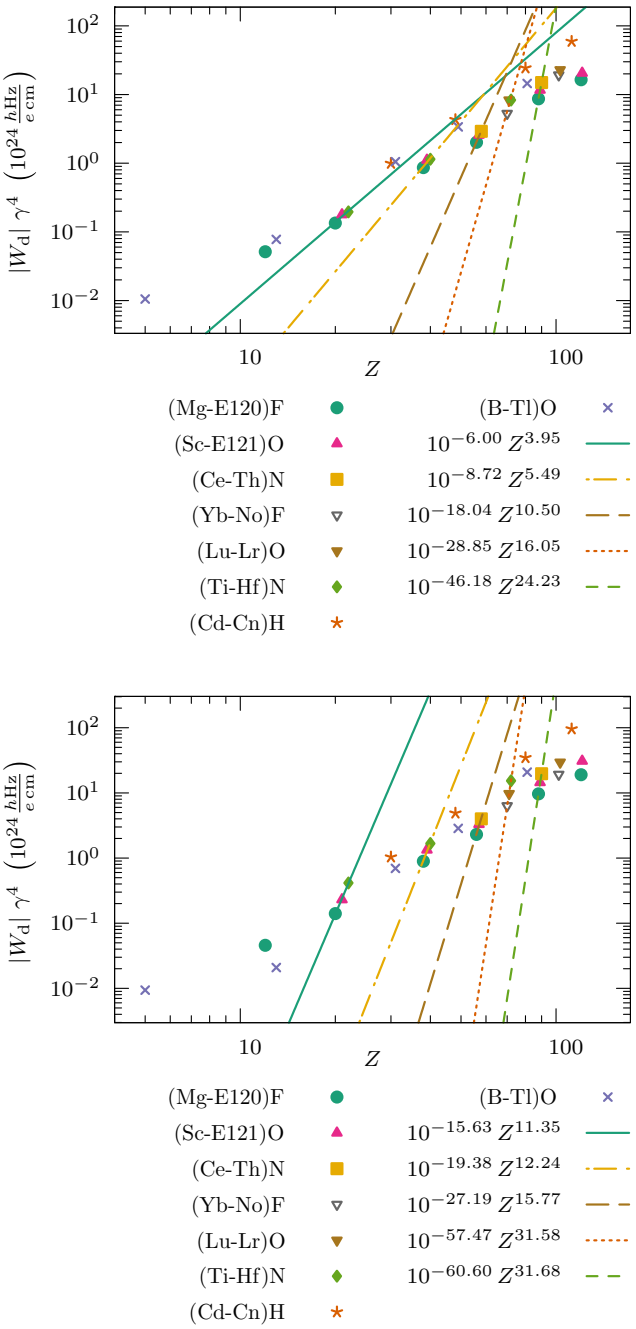

FIG. 8. Scaling of $\log_{10}\{|W_d|\gamma^4 \times 10^{-24}\,\frac{e\,\text{cm}}{h\text{Hz}}\}$ with $\log_{10}\{Z\}$ for row 4 (Ca-Ti; solid line), row 5 (Sr-Zr; dash-dotted line), row 6 (Ba-Ce; long-dashed line, Yb-Hf; dotted line), and row 7 (Ra-Th; short-dashed line) at the level of GKS-ZORA/B3LYP (top) and GHF-ZORA (bottom).

TABLE V. Z-scaling a and Z-independent factors b of $\frac{|W_s|}{R(Z,A)f(Z)^{\frac{\gamma+1}{2}}}$ and $|W_d|\gamma^4$ for isolobal diatomic molecules in row 4 (Ca-Ti), row 5 (Sr-Zr), row 6 (Ba-Ce; Yb-Hf), and row 7 (Ra-Th) at the level of GHF/GKS-ZORA. Standard uncertainties of the fit are given in parentheses with respect to the last or two last significant digits.

	a_s		b_s		$a_{d,FS}$		$b_{d,FS}$	
Row	GHF	GKS	GHF	GKS	GHF	GKS	GHF	GKS
4 (Ca-Ti)	11.6(8)	4.1(11)	−15.8(11)	−6.1(14)	11.3(7)	3.9(11)	−15.6(9)	−6.0(15)
5 (Sr-Zr)	12.2(16)	5(2)	−19(3)	−8(4)	12.2(19)	5(3)	−19(3)	−9(4)
6 (Ba-Ce)	16(3)	11(2)	−28(5)	−18(4)	16(3)	10.5(19)	−27(5)	−18(3)
6 (Yb-Hf)	31.7(11)	15(9)	−58(2)	−27(17)	31.6(7)	16(9)	−57.5(14)	−29(17)
7 (Ra-Th)	33(2)	24.9(10)	−62(4)	−47(2)	32(2)	24.2(12)	−61(5)	−46(2)

discussing eEDM enhancement we concentrate on the results obtained with the empirical relativistic enhancement factor in the following. For comparison, results obtained from the analytically derived relativistic enhancement factor are provided in the Supplemental Material [46]. The corresponding plots can be found in Fig. 7 for W_s and Fig. 8 for W_d and the resulting scaling and damping parameters are listed in Table V.

Trends, similar to those reported in [47] for the $\mathcal{P}$-odd nuclear spin-dependent interaction can also be observed for the $\mathcal{P},\mathcal{T}$-odd properties. However, we can see a large discrepancy ($\gtrsim$20% for parameter a and b) between results obtained from GHF and GKS calculations. Deviations for a and b of more than 50% between the GHF and GKS results in the fourth and fifth row probably stem from electron correlation effects, which lead to a considerable reduction (of 30% to 50%) of the enhancement effects in group 4 compounds. Fits of the DFT results have large errors that lead to qualitative differences. Especially for row 6 compounds with a filled f shell (violet line in Figs. 7 and 8) a large fit error (>40%) can be observed, since HfN does not fold into the power-law model. The results of GHF fit much better into this model and show that the scaling behavior of post-f-block compounds of row 6 is approximately similar to that of row 7 compounds without a filled f shell. Comparing compounds with a filled d shell (group 12 and 13), we see that the slope becomes negative. This again indicates a maximum of enhancement of $\mathcal{P},\mathcal{T}$-odd effects in group 12 as discussed before.

The investigations show that the chemical environment of the heavy atom can have a much more important effect on the Z-dependent enhancement than the physical nature of the atom. This can result in effects scaling as $\sim 10^b Z^{30}$ for row 7 compounds. Thus a more complex chemical environment may allow for better tuning of the size of $\mathcal{P},\mathcal{T}$-odd enhancement effects. Hence we may speculate that polyatomic molecules might be capable to give larger enhancement effects due to the electronic structure surrounding the heavy atom.

V. CONCLUSION

In this paper we calculated $\mathcal{P},\mathcal{T}$-odd properties due to eEDM and nucleon-electron current interactions in polar open-shell diatomic molecules. We determined periodic trends of $\mathcal{P},\mathcal{T}$ violation by comparison to atomic scaling relations and showed that the trends are very similar to those of nuclear spin-dependent $\mathcal{P}$-violating interactions. Furthermore, this comparison revealed problems of frequently used scaling relation for eEDM enhancement in the regime of heavy elements with $Z > 100$. We showed that an alternative relativistic enhancement factor found empirically by Fermi and Segrè resolves the problems for $Z < 137$ partially. Group 12 hydrides and group 4 nitrides were identified to show a very steep Z scaling and therefore interesting Z-dependent electronic structure effects, enhancing $\mathcal{P},\mathcal{T}$ violation in these compounds, were identified. Furthermore, a study of the ratio between $\mathcal{P},\mathcal{T}$-odd properties W_d/W_s, showed that electronic structure effects and the chemical environment have a very small influence on the ratio. The ratio is mainly determined by an exponential dependence on the nuclear charge Z. Thus for experiments aiming to differentiate between d_e and k_s, the use of molecules with a relatively large difference in nuclear charge Z would be favorable. The analysis of the scaling of isolobal systems and the study of the ratio W_d/W_s showed the limitations of polar diatomic molecules and point towards possible advantages in the use of more complex systems, such as polyatomic molecules. The latter will be focus of future research in our laboratory.

ACKNOWLEDGMENTS

Financial support by the State Initiative for the Development of Scientific and Economic Excellence (LOEWE) in the LOEWE-Focus ELCH and computer time provided by the Center for Scientific Computing (CSC) Frankfurt are gratefully acknowledged. T.I. is grateful to RFBR Grant N 16-02-01064 for partial support. S.M. gratefully acknowledges support from Fonds der Chemischen Industrie. We thank Yuri Oganessian for inspiring discussions on super heavy elements.

[1] D. J. Gross, Proc. Natl. Acad. Sci. USA **93**, 14256 (1996).
[2] N. Fortson, P. Sandars, and S. Barr, Phys. Today **56**, 33 (2003).
[3] I. B. Khriplovich and S. K. Lamoreaux, *CP Violation without Strangeness* (Springer, Berlin, 1997).

[4] J. S. M. Ginges and V. V. Flambaum, Phys. Rep. **397**, 63 (2004).
[5] E. Salpeter, Phys. Rev. **112**, 1642 (1958).
[6] P. Sandars, Phys. Lett. **14**, 194 (1965).
[7] P. G. H. Sandars, Phys. Lett. **22**, 290 (1966).
[8] P. G. H. Sandars, J. Phys. B **1**, 511 (1968).
[9] P. G. H. Sandars, J. Phys. B **1**, 499 (1968).
[10] V. K. Ignatovich, Sov. Phys. JETP **29**, 1084 (1969).
[11] V. V. Flambaum, Yad. Fiz. **24**, 383 (1976) [Sov. J. Nucl. Phys. **24**, 199 (1976)].
[12] I. B. Khriplovich, *Parity Nonconservation in Atomic Phenomena* (Gordon and Breach, Philadelphia, PA, 1991).
[13] V. S. Prasannaa, A. C. Vutha, M. Abe, and B. P. Das, Phys. Rev. Lett. **114**, 183001 (2015).
[14] A. Sunaga, M. Abe, M. Hada, and B. P. Das, Phys. Rev. A **95**, 012502 (2017).
[15] B. Ravaine, S. G. Porsev, and A. Derevianko, Phys. Rev. Lett. **94**, 013001 (2005).
[16] K. Gaul and R. Berger, J. Chem. Phys. **147**, 014109 (2017).
[17] F. Hund, Z. Phys. **40**, 742 (1927).
[18] F. Hund, Z. Phys. **42**, 93 (1927).
[19] F. Hund, Z. Phys. **43**, 805 (1927).
[20] M. G. Kozlov and L. N. Labzowsky, J. Phys. B **28**, 1933 (1995).
[21] Y. Y. Dmitriev, Y. G. Khait, M. G. Kozlov, L. N. Labzowsky, A. O. Mitrushenkov, A. V. Shtoff, and A. V. Titov, Phys. Lett. A **167**, 280 (1992).
[22] E. Lindroth, B. W. Lynn, and P. G. H. Sandars, J. Phys. B **22**, 559 (1989).
[23] T. A. Isaev and R. Berger, arXiv:1302.5682.
[24] A. D. Kudashov, A. N. Petrov, L. V. Skripnikov, N. S. Mosyagin, T. A. Isaev, R. Berger, and A. V. Titov, Phys. Rev. A **90**, 052513 (2014).
[25] C. van Wüllen, J. Chem. Phys. **109**, 392 (1998).
[26] L. Visscher and K. G. Dyall, At. Data Nucl. Data Tables **67**, 207 (1997).
[27] A. Mårtensson-Pendrill and P. Öster, Phys. Scr. **36**, 444 (1987).
[28] E. Fermi and E. Segrè, Z. Phys. **82**, 729 (1933).
[29] M. A. Bouchiat and C. Bouchiat, J. Phys. (Paris) **35**, 899 (1974).
[30] O. P. Sushkov and V. V. Flambaum, Sov. Phys. JETP **48**, 608 (1978).
[31] G. Racah, Z. Phys. **71**, 431 (1931).
[32] T. H. Dinh, V. A. Dzuba, and V. V. Flambaum, Phys. Rev. A **80**, 044502 (2009).
[33] E. Fermi and E. Segrè, Mem. Accad. d'Italia **4**, 131 (1933).
[34] G. Breit, Phys. Rev. **38**, 463 (1931).
[35] V. A. Dzuba, V. V. Flambaum, and C. Harabati, Phys. Rev. A **84**, 052108 (2011).
[36] R. Berger, J. Chem. Phys. **129**, 154105 (2008).
[37] R. Berger and C. van Wüllen, J. Chem. Phys. **122**, 134316 (2005).
[38] R. Berger, N. Langermann, and C. van Wüllen, Phys. Rev. A **71**, 042105 (2005).
[39] T. A. Isaev and R. Berger, Phys. Rev. A **86**, 062515 (2012).
[40] S. Nahrwold and R. Berger, J. Chem. Phys. **130**, 214101 (2009).
[41] R. Ahlrichs, M. Bär, M. Häser, H. Horn, and C. Kölmel, Chem. Phys. Lett. **162**, 165 (1989).
[42] P. J. Stephens, F. J. Devlin, C. F. Chabalowski, and M. J. Frisch, J. Phys. Chem. **98**, 11623 (1994).
[43] S. H. Vosko, L. Wilk, and M. Nuisar, Can. J. Phys. **58**, 1200 (1980).
[44] A. D. Becke, Phys. Rev. A **38**, 3098 (1988).
[45] C. Lee, W. Yang, and R. G. Parr, Phys. Rev. B **37**, 785 (1988).
[46] See Supplemental Material at http://link.aps.org/supplemental/10.1103/PhysRevA.99.032509 for details on the used basis sets and further plots of trends derived with the analytical relativistic enhancement factor by Sandars.
[47] T. A. Isaev and R. Berger, J. Mol. Spectrosc. **300**, 26 (2014).
[48] B. O. Roos, R. Lindh, P. k. Malmqvist, V. Veryazov, and P. O. Widmark, J. Phys. Chem. A **108**, 2851 (2004).
[49] T. H. Dunning, Jr., J. Chem. Phys. **90**, 1007 (1989).
[50] W. Liu, C. van Wüllen, F. Wang, and L. Li, J. Chem. Phys. **116**, 3626 (2002).
[51] Y. T. Oganessian, V. K. Utyonkov, Y. V. Lobanov, F. S. Abdullin, A. N. Polyakov, R. N. Sagaidak, I. V. Shirokovsky, Y. S. Tsyganov, A. A. Voinov, G. G. Gulbekian, S. L. Bogomolov, B. N. Gikal, A. N. Mezentsev, S. Iliev, V. G. Subbotin, A. M. Sukhov, K. Subotic, V. I. Zagrebaev, G. K. Vostokin, M. G. Itkis, K. J. Moody, J. B. Patin, D. A. Shaughnessy, M. A. Stoyer, N. J. Stoyer, P. A. Wilk, J. M. Kenneally, J. H. Landrum, J. F. Wild, and R. W. Lougheed, Phys. Rev. C **74**, 044602 (2006).
[52] Y. Oganessian, A. Yeremin, G. Gulbekian, S. Bogomolov, V. Chepigin, B. Gikal, V. Gorshkov, M. Itkis, A. Kabachenko, V. Kutner, A. Lavrentev, O. Malyshev, A. Popeko, J. Roháč, R. Sagaidak, S. Hofmann, G. Münzenberg, M. Veselsky, S. Saro, N. Iwasa, and K. Morita, Eur. Phys. J. A **5**, 63 (1999).
[53] Y. Oganessian, J. Phys.: Conf. Ser. **312**, 082003 (2011).
[54] V. K. Utyonkov, N. T. Brewer, Y. T. Oganessian, K. P. Rykaczewski, F. S. Abdullin, S. N. Dmitriev, R. K. Grzywacz, M. G. Itkis, K. Miernik, A. N. Polyakov, J. B. Roberto, R. N. Sagaidak, I. V. Shirokovsky, M. V. Shumeiko, Y. S. Tsyganov, A. A. Voinov, V. G. Subbotin, A. M. Sukhov, A. V. Karpov, A. G. Popeko, A. V. Sabel'nikov, A. I. Svirikhin, G. K. Vostokin, J. H. Hamilton, N. D. Kovrizhnykh, L. Schlattauer, M. A. Stoyer, Z. Gan, W. X. Huang, and L. Ma, Phys. Rev. C **97**, 014320 (2018).
[55] M. Jung, J. High Energy Phys. 05 (2013) 168.
[56] T. Chupp and M. Ramsey-Musolf, Phys. Rev. C **91**, 035502 (2015).
[57] T. Fleig, Phys. Rev. A **96**, 040502 (2017).
[58] JCGM 102:2011, Evaluation of measurement data—Supplement 2 to the Guide to the expression of uncertainty in measurement—Extension to any number of output quantities, Standard (Joint Committee for Guides in Metrology, Paris, FR, 2011).
[59] T. Fleig and M. Jung, J. High Energy Phys. 07 (2018) 12.
[60] A. Borschevsky, M. Ilias, V. A. Dzuba, V. V. Flambaum, and P. Schwerdtfeger, Phys. Rev. A **88**, 022125 (2013).
[61] P. Pyykkö and J. P. Desclaux, Acc. Chem. Res. **12**, 276 (1979).
[62] C. Thierfelder and P. Schwerdtfeger, Phys. Rev. A **82**, 062503 (2010).